Ph.D. DISSERTATION

AC biasing for electrical detection of biomolecules

(교류 신호를 이용한 생체 분자의 전기적 검출에 관한 연구)

By

Seok Hyang Kim

August 2015

SCHOOL OF ELECTRICAL ENGINEERING AND COMPUTER SCIENCE
COLLEGE OF ENGINEERING
SEOUL NATIONAL UNIVERSITY

AC biasing for electrical detection of biomolecules

(교류 신호를 이용한 생체 분자의 전기적 검출에 관한 연구)

指導敎授 朴 榮 俊

이 論文을 工學博士 學位論文으로 提出함

2015 年 8 月

서울大學校 大學院

電氣–컴퓨터 工學部

金 錫 享

金 錫 享의 工學博士 學位論文을 認准함

2015 年 8 月

委 員 長 _____ (印)
副委員長 _____ (印)
委 員 _____ (印)
委 員 _____ (印)
委 員 _____ (印)

AC biasing for electrical detection of bio molecules

by

Seok Hyang Kim

Submitted to the School of Electrical Engineering and
Computer Science
in partial fulfillment of the requirements for the degree of
Doctor of Philosophy in Electrical Engineering
at
SEOUL NATIONAL UNIVERSITY
August 2015

Committee in Charge:

Sunghoon Kwon, Chairman
Young June Park, Vice-Chairman
Sung Jae Kim
Junho Chung
Jungbae Kim

Abstract

In various medical and biological applications, the label-free (i.e., electrical) detection of charged biomolecules such as DNA/RNA and proteins offers a number of advantages over the well-established optical methods. Electrical nanobiosensors, in particular, have additional advantages in terms of speed of sensing, accuracy of detection, and the possibility of semiconductor device integration. However, degradation of the signal due to nonspecific binding with background molecules reduces the sensitivity and selectivity of the electrical biosensor and has prevented its successful application.

In this dissertation, I propose to study the electrochemical reaction that takes place between the target and probe molecules to enhance the association rate constant and between the biomolecules and the surface of a carbon nanotube (CNT) to suppress the adsorption of nonspecific biomolecules in serum throughout the experiment and the numerical result of the simulation.

For the enhancement of the association rate constant between the probe and the target molecules, the specific pulse train applied to the device consists of the carbon nanotube network channel formed on the concentric electrodes. In order to optimize the association efficiency, various input conditions are considered for DNA hybridization experiments (i.e., frequency, size of the gold nanoparticle, and the ionic strength of the electrolyte). Compared with the DC and non-biasing conditions, the pulse-biasing method offers better selectivity and sensitivity enhancement in a buffer solution to detect the dengue virus–specific DNA sequence, and a very low limit of detection can be achieved in serum.

To suppress the adsorption of nonspecific binding of biomolecules in serum, the specific pulse train is applied to the device. There is no need for an additional CNT surface treatment (e.g., Tween-20, polyethylene glycol [PEG], or the like) and no additional washing step for the nonspecific binding of biomolecules in serum owing to the systematic factor change such as the concentration of hydrogen ion and dynamic

motion of the biomolecules through the electric field. Each moment of signal change from positive bias to negative bias or from negative bias to positive bias could suppress the undesired binding event with nonspecific molecules.

This experiment and simulation using the pulsed-bias scheme can be extended to general electrical biosensor platforms for detecting DNA and proteins and to determine the optimal conditions for maximizing the sensitivity and selectivity of the sensor by considering the electrical characteristics of biomolecules.

Keywords: Pulsed Measurement, Affinity-Based Biosensor, DNA Hybridization, Selectivity, local pH.

Student Number: 2010-30212

Contents

List of Tables

List of Figures

Chapter 1

Introduction

1.1 Motivation and the historical review: Electrical nano bio sensor

A biosensor is an analytical device that converts biological reactions into measurable physiochemical signals which are transferred to detecting a change at a localized surface. The applications of biosensors are detection of various substances such as metabolites, pollutants, antimicrobial agents, gene therapy, and so on. The biosensor was first reported by Leland C. Clark in 1956, who is considered to be the

"father of biosensors" [1-3]. Although the concept of biosensors has been known since the late 20th century, their uses were limited to laboratory studies. With the advent of sciences, several modern biosensors were designed. Novel biochemical elements, such as aptamers and materials with molecular imprints, have been introduced into biosensor assemblies, and the family of DNA sensors has been added to traditional biosensors with specific goals such as the detection of oligonucleotides, proteins, and the low-molecular-weight compounds able to bind to DNA [4-7].

In order to have reliable diagnostic tools for the rapid detection and identification of biological agents, new methods should be developed that will permit label-free and real time measurement of simultaneous interactions. Biosensing devices, fabricated by means of nanotechnologies, are powerful devices that can fulfill these requirements and have the added draw of being portable, making "point-of-care (PoC)" analysis possible [8, 9].

Specifically, electrical nanobiosensors, a product of convergence technology, has emerged as one of the most promising candidates for overcoming the barriers to current medical needs such as single-molecule analysis, real-time detection, low power dissipation, and miniaturization for in vivo applications. In a biodetection platform, these devices can also offer the multiplex capability to identify biological agents more rapidly than can be achieved with routine clinical analysis [8, 10].

The general concept of electrical nano-biosensing by low-dimensional field-effect transistors (FETs) has been explored in studies of carbon nanotubes (CNT), silicon nanowire, nanocluster, and graphene devices [11-13]. Although different nanomaterials can be used as substrates, CNTs have enormous potential because they can act both as immobilization matrices and as electrochemical transducers simultaneously. In addition, CNTs are stable over a large range of potentials, are catalytically active toward many electrochemical reactions, and provide a significant increase in electrode area [14-16]. Since the discovery of CNTs [17], the impact on nanotechnology of this novel nano-sized material continues to grow with each passing year. Moreover, demand is increasing for the commercial utilization of this material in the industry, such as highly sensitive, miniaturized biochemical sensors.

However, electrical biosensors suffer from parasitic noise issues such as the noise from nonspecific target molecules. Degradation of the signal due to nonspecific binding with background molecules and the charge screening effect due to ions within the electrical double layer (EDL) have been the roadblocks to success of the electrical biosensor [18-21]. Sometimes washing the sensor before readout can reduce this nonspecific binding by washing away the adsorbed molecules while leaving the probe–target binding; however, for real-time measurement during the PoC application, this washing step should be avoided [22-24]. Therefore, a more effective method for achieving higher-sensitivity detection within a rapid timeframe

is in great demand.

This thesis explains, possible ways to overcome the general challenges posed by the FET-based electrical biosensor chip for practical applications. These challenges are the degradation of the electrical signal due to nonspecific binding of biomolecules and a low affinity efficiency between the probe and the target biomolecules; also, selectivity is degraded by the noisy molecules included in the real samples (such as serum). In Sections 1.2 and 1.3, I briefly introduce issues in the electrical biosensor and selectivity enhancement method with our platform.

1.2 Issues in the electrical biosensor

The selectivity and sensitivity are critical issues limiting the biosensor performance [25]. The selectivity issues is related to the probe-target binding efficiency [26, 27] and nonspecific binding, in which non-target bio molecules stick to the probe layer, preventing target binding, or causing a false positive signal. Specifically, electrical biosensors are expected to response only to the target molecule, and not to other similar molecules, called noisy molecules. However, an electrical biosensor cannot, in general, distinguish a probe-target binding signal from a probe-noisy molecule binding event. For example, the detection of low-abundant target molecules (under ng/mL) [28, 29] in human serum (~70 mg/mL in total protein content) is one of the greatest challenges in the biosensor field. On the other hand, the sensitivity issue is related to the limit of detection (LOD) and the signal-to-noise ratio.

In this study, we apply an electrical pulse bias between the electrical channel, to which the probe molecules are attached, and the electrolyte, containing the target molecules, during the hybridization event. The method provides two important improvements: (i) enhancing the hybridization rate, and (ii) enhancing the selectivity of the electrical biosensor. Firstly, the hybridization rates between the probe and target molecules are significantly improved, due to the mechanical oscillations of the probe and target molecules, caused by the external electric field around the charged

probe molecules.

Secondly, it is possible to suppress the adsorption of nonselective proteins in serum such as albumin, thereby enhancing the selectivity of the electrical biosensor. The suppression of the nonspecific binding under the pulse train is due to the unsymmetrical field force experienced by the protein during the pulse transitions (high to low and low to high) and the non-symmetry is caused by the different transient times between the electric field and the charge/discharge of the protein according to the surface pH modulation in serum.

1.3 AC bias scheme

1.3.1 Composition for pulsed measurement

The schematics of the pulse voltage train applied to the drain electrode (island) as V_{in} during the hybridization events between the probe DNA (p-DNA) and target DNA (t-DNA), are shown in Fig. 1-1. Though one could apply various types of AC biasing, such as wave, triangle and saw-tooth, we have used the step profile only, because it can tell the steady-state current value, while other types of profiled do not have an inherently steady state.

The electrical signal of carbon nanotube networks (CNN) on the test pattern was measured using the electrical set up to implement the pulse bias scheme as shown in Fig. 1-1. This system consist of the prepared sensor array device, the pulse generator

(Tektronix AFG3021), the operational amplifier and the oscilloscope (Tektronix DPO7104) for the signal observation. The pulse trains with positive and negative amplitude applied to the island electrode (drain) as V_{in} (1 kHz, ±0.5 V). The real time measurement under the consecutive pulse biasing during the experiment collects the output voltage in the steady state as shown in Fig. 1-1.

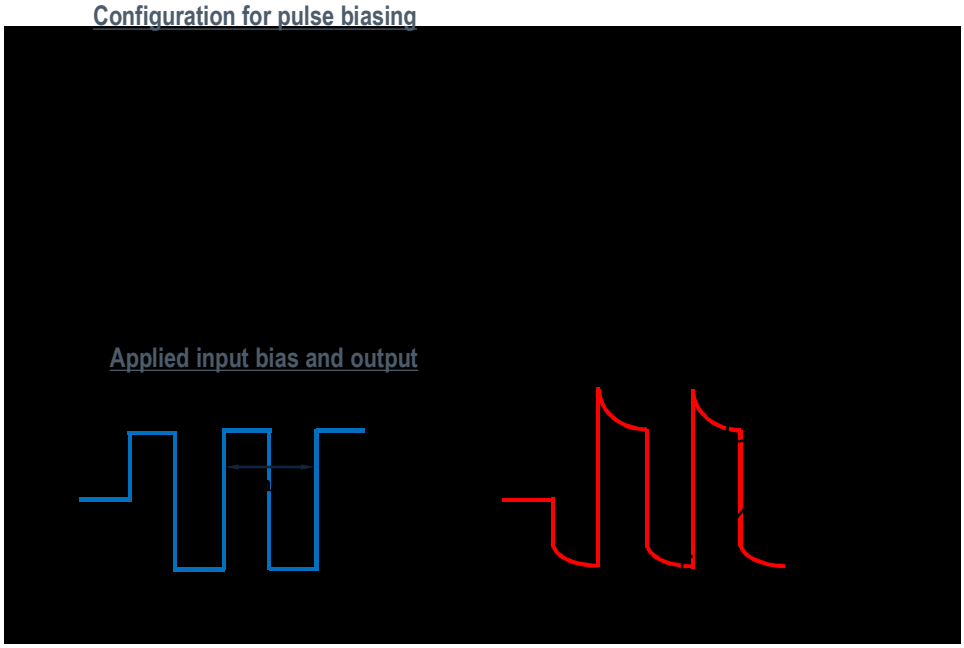

Fig. 1-1. (a) The equivalent circuit diagram of the CNT network (CNN) device with the electrical measurement setup. (b) Applied pulse biasing to the drain electrode and the output voltage of the OP amplifier, which is proportional to the channel and charging current.

1.3.2 RC time constant of the sensor system (simulation & experiment)

When a pulse bias is applied to the sensor system that includes an electrolyte solution, ions forming EDL are redistributed, according to the applied bias condition. The time required to reach the steady state is determined by τ_{RC}, which is related to the mobility, and the concentration of the ions within the electrolyte solution [30]. The mobility of the ions in the electrolyte solution is significantly lower than that of the electrons and holes in the semiconductor, thus the τ_{RC} of the sensor system is ~ O(1) micro-seconds under the assumption that the phosphate buffered saline (PBS) contains NaCl (100 mM).

The redistribution of the EDL ion is related to the RC constants of the whole system consisting of the electrode, electrolyte and CNN channel, so that the whole system should be considered, to estimate the time response. Fig. 1-2 (a) shows the equivalent circuit, which consists of pMOSFET, R_i, C_i, representing the CNT network, resistances of the electrolyte solution, and the capacitances of EDL, respectively.

Each parameter used in the equivalent circuit is described by the following equations.

$$R_i = \rho_{buffer} \frac{l_i}{s_i}, \tag{1.1}$$

where, R_i is the buffer solution (NaCl concentration of 100 mM) resistance (i = D,

G, S), ρ_{buffer} (1.067 ohm · m) is the Buffer solution resistivity, l_i is the distance between the top of the electrolyte droplet and each node in the electrode and channel, and s_i is the cross-sectional area of each node. The EDL capacitance per unit area, C_0 is expressed as

$$C_0 = \sqrt{\frac{2n_0\varepsilon\varepsilon_0 z^2 e^2}{kT}\cosh\left(\frac{ze\varphi_0}{2kT}\right)}, \tag{1.2}$$

where, $\varepsilon\varepsilon_0$ is the deionized (DI) water permittivity, n_0 is the number density of the ionic species (NaCl: 100 mM), and φ_0 is the electric surface potential. Since the surface area of the source electrode is much greater than the surface area of the drain electrode, we set $C_S \approx 1000 C_D$, under the assumption that the area of the source electrode is 1000 times larger than the drain electrode area.

The results from the equivalent circuit were validated using the I_{DS}-V_{DS} curve with experimental measurements, as shown in Fig. 1-2 (b). Fig. 1-2 (c) shows the transient measurement results for experiment and simulation in the PBS. The time duration for the initial transient behavior is defined by the time constant, τ_{RC}, and it can be estimated as ~ O(1) micro-seconds, under the assumption that the PBS contains NaCl (100 mM). Experimental data show slightly incremental behavior after τ_{RC}, but the transient current should be measured within τ_{RC}, so that the increasing time part can be neglected.

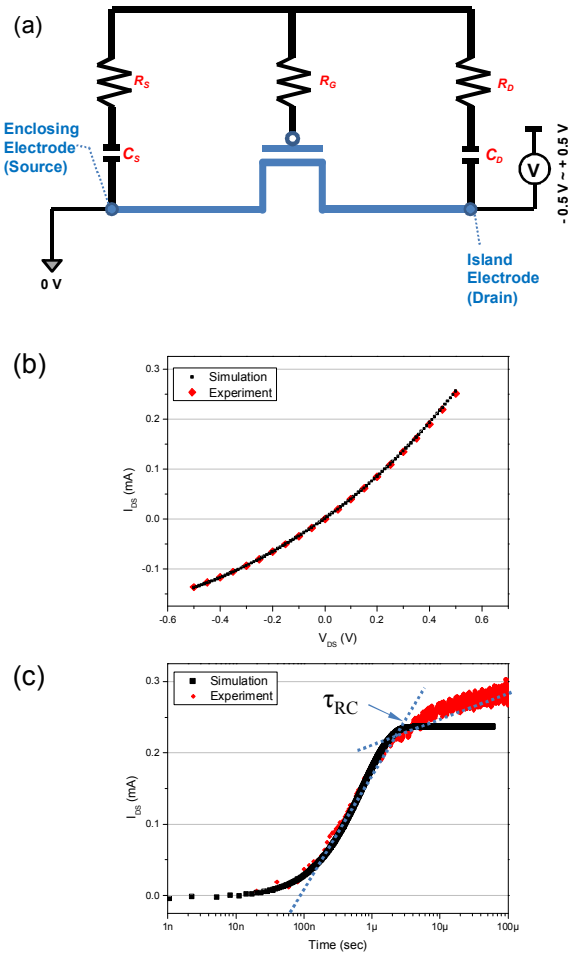

Fig. 1-2. (a) Equivalent circuit for the CNN system in the buffer solution. (b) *I-V* characteristics of the CNN channel from simulation and measurement. (c) Transient behavior of the drain current, after the unit step of 0.5 V is applied to the drain, from simulation and measurement.

1.4 Outline of the Dissertation

This dissertation is organized as follows.

In chapter 2, CNT platform (M1 chip used in this experiment) for DNA sensing is described. The test pattern manufacturing process for the M1 device fabrication and the post processing for the CNT channel formation, the Au nano particle deposition are described.

In chapter 3, effects of the AC biasing during DNA hybridization to detection of dengue fever specific sequence DNA is shown. The selectivity enhancement method adopting the pulse bias scheme has been introduced and experimentally verified by the DNA detection using the CNN-gold nano particle (GNP) FET sensors. Also, it has been shown that a LOD of as low as ~pM concentration can be achieved, in the detection of DNA in the serum conditions.

In chapter 4, represents the concepts of the electrical passivation and electronic modulation of local pH of buffer solution in CNN device. It is found that the local pH is modulated at the CNT and buffer solution interface by electrical pulse. The effect of modulated surface pH, thereby the charge state of the defects on the CNT, on the device operation with the CNT channel is quantitatively predicted and verified by the experiments.

In chapter 5, electrical passivation of nonselective bio molecules in CNN device is shown. We present an experimental and simulation study about desorption of

albumin, a representative nonselective molecules in serum, on CNT surface as an electrical bio sensing channel under the pulse train condition. To theoretically model the behavior of molecules and ions under the step pulse bias, the physics on the reaction rate, mass transport and the resulting surface pH-value are considered using the Poisson and drift-diffusion equations.

In chapter 6, conclusions and suggestions for the further works are given.

Chapter 2

Experimental platform: (M1 chip with the carbon nanotubes as the electrical channel) for DNA sensing

2.1 Introduction

In this chapter, test samples, fabrication methods, and basic electrical properties of the fabricated CNN devices will be presented. The concentric electrode structure has been formed by the conventional one-metal process [31]. The channel consisting

of the CNN and GNP can be fabricated by CNT dip-coating, and physical evaporation of Au, respectively [32]. The concentric electrode structure provides an interesting feature called the “self-gating effect” [33]. The effect can be elaborated as the electrical potential of an electrolyte solution applied on the sensor platform being generally determined by the potential of the enclosing (source), which has much large are, due to the capacitance ratio (1000:1 in this work). Applying the drain bias to the island (drain) electrode, the conductance of the CNN channel between two electrodes can be modulated by the electrolyte gating, resulting from the reset bias value at the enclosing electrode. In other words, the electrolyte gating effect can be obtained in our sensor array platform, without any external gate electrode.

2.2 Sensor device preparation

The test chips (M1), having a concentric electrode structure were fabricated at the Inter-university Semiconductor Research Center (ISRC) of Seoul National University, using a conventional one-metal process, which consisted of Ti/Au as a metal. After deposition of the 50 nm thick Ti on top of the thermally grown SiO_2 with a thickness of 1μm, a 15 μm channel length is formed by the liftoff process of Au layer with a thickness of 200 nm.

The first step of post processing is a dip-coating of single-walled CNT (swCNT).

The swCNTs (ASP-100F produced by Il-jin Nanotech, Korea) were ultrasonicated in nitric acid at 50 °C for 30 min to purify and simultaneously exfoliate from bundles. The swCNTs are then neutralized with deionized (DI) water and trapped on the membrane filter (Millipore, 0.2 μm pore size, 47 mm diameter) by a vacuum filtration method. The swCNTs on the filter were dried in a vacuum oven chamber at 80 °C for 48h. The prepared swCNTs were dispersed in 1,2-dichlorobenzene solution with a concentration of 0.05 mg/mL, and then an ultrasonication process is performed for 10 h. For the channel formation between the two electrodes, the fabricated chip was immersed in a swCNT colloidal solution and pulled out at a constant withdrawal velocity of 3.0 mm/min. During the dip-coating, swCNT bundle was deposited on the surface of the oxide surface in the form of a network. The diameter of the nanotubes, measured using an atomic force microscope, appears to be less than 1.5 nm, indicating that they are mostly single-walled.

The second step of post processing is Au deposition on the swCNT to provide a docking place for the probe molecules and to enhance the attachment of the swCNT to the Au electrode during the overall swCNT sensor device integration. Deposition of GNP on swCNT network was performed by thermal evaporation method. The deposition rate and thickness was monitored using a quartz crystal microbalance (QCM). The diameter of Au on the swCNT was about 7 nm. After deposition of GNP, the fabricated chip was annealed at 350 °C about 30 min for enhancing GNP

attachment to swCNT network. We will call a carbon nanotube network with Au particles as CNN-GNP.

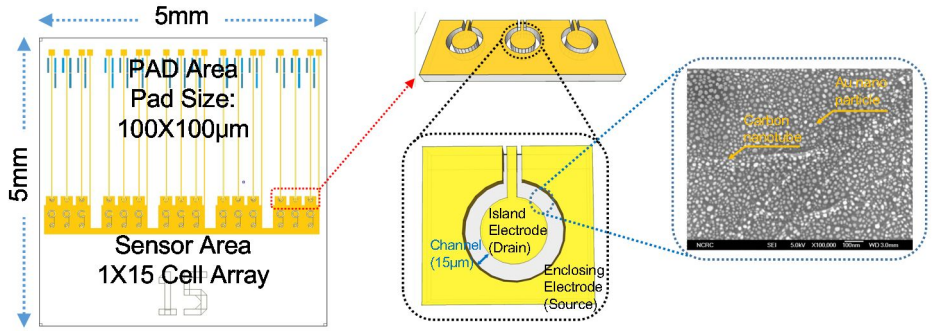

Fig. 2-1. Conceptual diagram of sensor array, and structure of individual sensor device. Concentric structure consists of drain and source electrode in electrolyte which gives self gating effect.

2.3 The ohmic contact between the Au electrode and CNT

We have employed an Au electrode, which has a large work function (~ 5.1 eV) as shown in Fig. 2-2 (a), for an improvement of the contact property. Fig. 2-2 (c) shows the typical *I-V* characteristics of a CNN device, with the Au electrode system shown in Fig. 2-2 (b). This result leads to a conclusion that the contact between the Au electrode and the CNT is an Ohmic contact. If one uses a low work function material, such as Al, the $R_{contact}$ in Fig. 2-2 (b) should be carefully considered.

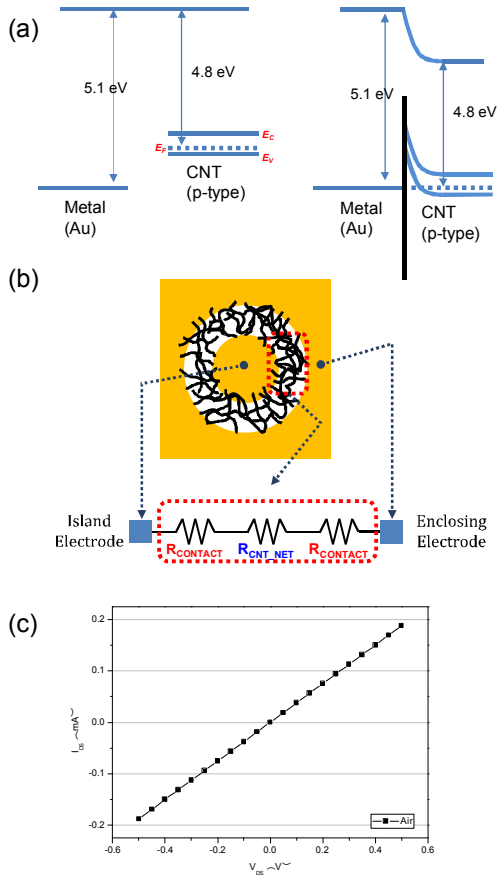

Fig. 2-2. (a) Suggested band diagram of the device. The CNT with a work function of ~4.8 eV is connected to an Au electrode. Owing to the difference in work function between the CNT and the Au, ohmic contact can be obtained. (b) Conceptual scheme of the CNN channel between the island electrode and enclosing electrode. (c) The *I-V* curve was taken with the voltage applied to drain from –0.5 V to +0.5 V, and the source is 0 V. The conductance through electrode-CNT leads to ohmic behavior.

2.4 Details of the self-gating effect [33]

Fig. 2-3 (a) and (b) shows the schematics diagram of the bare CNN device and its equivalent circuit which is basically a two-terminal resistor with the electrolyte droplet as the gate. While the electrolyte gate is floated, however, it is capacitively coupled with the island electrode (drain) and enclosing electrode (source). The electrostatic potential of the electrolyte follows the potential of the source as the source-electrolyte capacitance is much larger than the drain-electrolyte capacitance ($C_S >> C_D$). Notice that the butting area between the electrolyte and source is much larger than that between the electrolyte and drain. The source electrode is shared with other devices.

The unique asymmetric feature of two electrodes system is manifested as the asymmetric current versus voltage *(I-V)* characteristics between two electrodes. We have previously reported this "*self gating effect*" using a unique biosensor architectures consisting of two gold electrodes with concentric structures [33]. Fig. 2-3 (c) shows the *I-V* characteristics of a representative bare CNN device in which the drain voltage is swept from –0.5 V ~ to +0.5 V, while the source voltage is fixed at 0 V. Due to the aforementioned *self gating effect*, the measured current shows well known asymmetric behavior with respect to the polarity of the V_{DS}. It is the diode characteristic for positive V_{DS} and the saturation pMOSFET characteristic for

negative V_{DS}. Notice here that our CNN channel is a p-type semiconductor with positive threshold voltage.

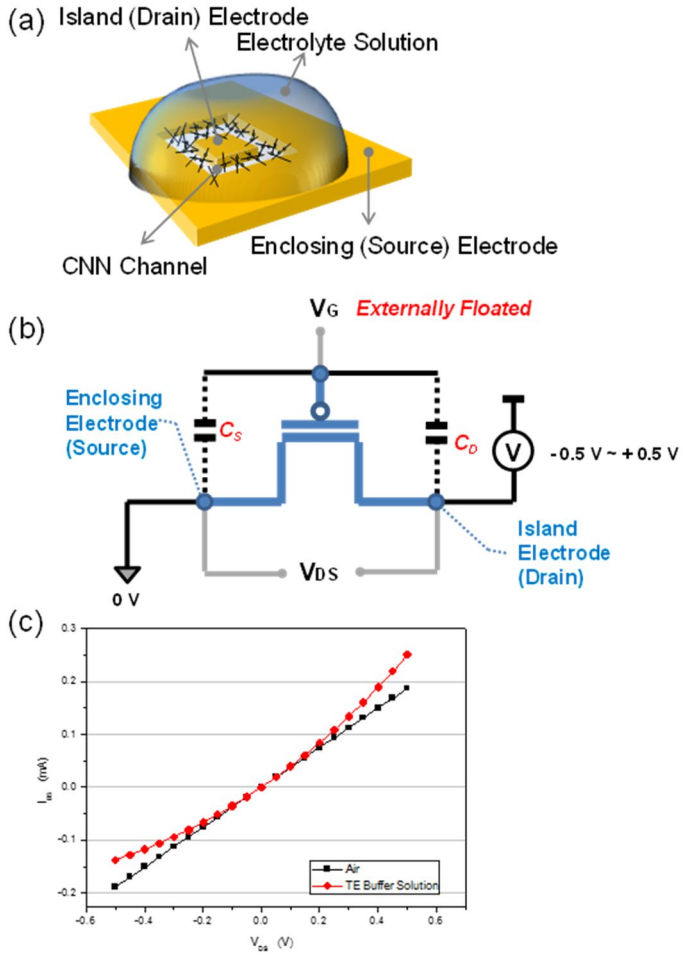

Fig. 2-3. (a) The schematics of concentric structure. (b) The equivalent circuit diagram of the concentric structure which has two electrodes. (c) The current versus voltage characteristics of a CNN fabricated on concentric structure with the floated gate.

Chapter 3

Effects of AC biasing on the DNA hybridization events

3.1 Introduction

In various medical and biological applications, the label-free (or electrical) detection of the charged bio molecules such as DNA/RNA and proteins has s number of advantages over the well-established optical methods [10, 25, 34]. However, the degradation of the signal due to nonspecific binding with the background molecules and the charge screening effect due to the ions within the EDL have been the roadblocks for the success of the electrical biosensor [18-21]. And washing the sensor before readout can reduce the nonspecific binding by washing away the adsorbed molecules while leaving the probe-target binding. But in the real-time measurement for the PoC application, this washing step should be

avoided [22-24]. There, a more effective method to achieve higher-sensitivity detection on a rapid timescale is in great demand.

In the following sections, we investigate the effect of the electrical pulse bias on detecting for charged bio molecules using CNT integrated bio sensor platform. Especially, the method described here represents an important improvement that allows highly selective detection of DNA in serum during hybridization. One major advantage of this approach is that it requires no additional CNT surface treatment [35, 36] (e.g., Tween-20, PEG, or the like) and no additional washing step to prevent the nonspecific binding of biomolecules in the serum.

3.2 Optimize the DNA hybridization condition

In order to optimize the association efficiency, various input conditions (frequency, GNP size, ionic strength of electrolyte) are considered for DNA hybridization experiments.

For an application of this sensor array to DNA sensing, thiolated 27-mer p-DNA molecules are immobilized on the GNP, as shown in Fig. 3-1. The immobilization of p-DNA was treated at room temperature overnight. And, the immobilized p-DNA samples were washed with PBS, for removal of nonspecific bound molecules.

It should be emphasized here that an alternating electrical field can easily be applied between the p-DNA molecules and the electrolyte, thanks to the electrode structure shown in Fig. 3-1, since the electrical potential of a bulk electrolyte is relatively stable.

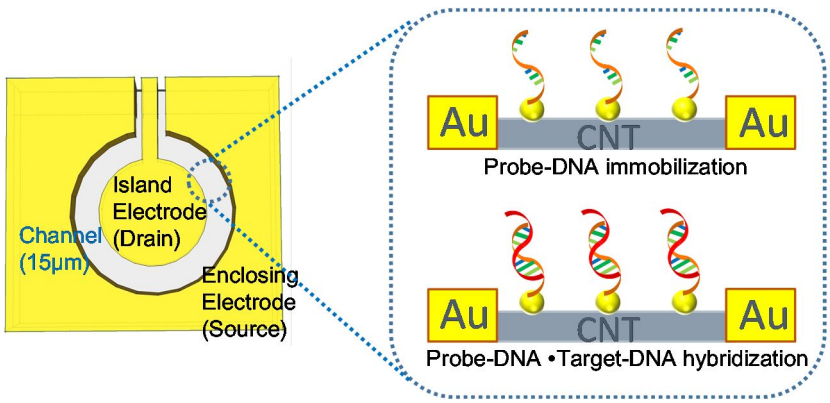

Fig. 3-1. Conceptual diagram of the CNT device. The CNN with Gold Nano Particles (GNP) is integrated between the concentric electrodes. Thiolated probe DNA (p-DNA) is immobilized on GNP, and bound with complementary t-DNA.

3.2.1 Effects of the AC frequency

After the PBS containing complementary t-DNA is applied to the sensor array device, the pulse bias at various frequencies is applied to a specific sensor device, with the other devices remain unbiased, for comparison. The electric potential applied to the island electrode is in the range from –0.5 V to +0.5 V, where the electrode oxidation-reduction reaction with ions hardly occurs [37]. Also, the conductivities of electrolyte (NaCl: 100 mM) and CNN are O(10^{-3}) S/cm, O(10) S/cm, respectively [38, 39]. Thus, the unwanted current between the island electrode and the enclosing electrode can be neglected, compared with the channel current.

Fig. 3-2 shows the sensitivity enhancement as a function of pulse frequency (±0.5 V in amplitude and 10 Hz, 100 Hz, 1 kHz, 10 kHz, 100 kHz in frequency). The sensitivity data less than 10 Hz was almost the same as the case for DC bias, and the frequency over 100 kHz may not be appropriate, since the measurement should be performed within the RC time constant of the whole system (O(1) micro-seconds). Notice that we need to measure the current after the steady state is reached in pulse duration during the hybridization event, in order to see the pure effect on the hybridization event. In this sense, there should be an optimum frequency value for maximizing binding efficiency, which is likely to be a function of DNA length. In our case, frequency near 1 kHz turns out to give the maximum sensitivity, as shown in Fig. 3-2.

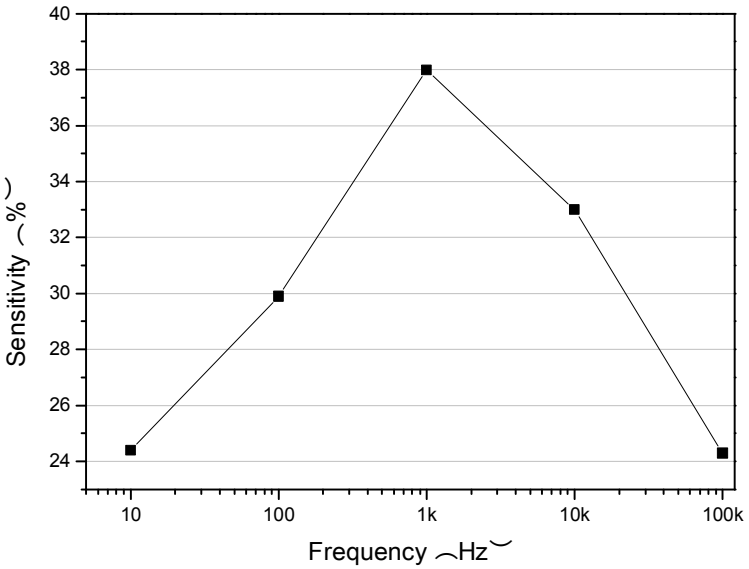

Fig. 3-2. Sensitivity data for 5 different frequencies of the pulsed bias signal applied during hybridization with the complementary t-DNA. The pulse is of ±0.5 V in amplitude, and 10 Hz, 100 Hz, 1 kHz, 10 kHz, 100 kHz in frequency.

3.2.2 Effects of the electrolyte ionic strength on DNA hybridization

The salt concentration of buffer solution is adjusted with NaCl giving final concentrations from 1 mM to 100 mM. The pulse voltage with ±0.5 V amplitude and 1 kHz frequency is applied to the drain electrode during the DNA hybridization. Fig. 3-3 shows the real time measurement data during the DNA hybridization. All sensor devices initially contain the complementary t-DNA of 5 μM concentration for each buffer concentration of 1 mM, 10 mM and 100 mM. Compared with the device with the t-DNA in diluted buffer solution condition (1 mM and 10 mM), the sensitivity and response time with the t-DNA in 1× buffer solution (~100 mM) shows improvement. After 500 sec in DNA hybridization, the conductance of the device in 1× buffer solution decreases by 37 %, while the conductance of the device in diluted buffer solution decreases by approximately 33 % (NaCl:10 mM), 23 % (NaCl:1 mM). We have estimated the time constants from the exponential fitting of real time hybridization measurements for both 1× buffer solution and diluted buffer solutions, leading 82 sec for 1× buffer, 179 sec (NaCl:10 mM) and 221 sec (NaCl:1 mM). The trend of results is due to screening of electrostatic penalties (lower electrolyte concentration → longer screening length → preventing the binding between probe and target) to hybridization at lower ionic strengths [40, 41].

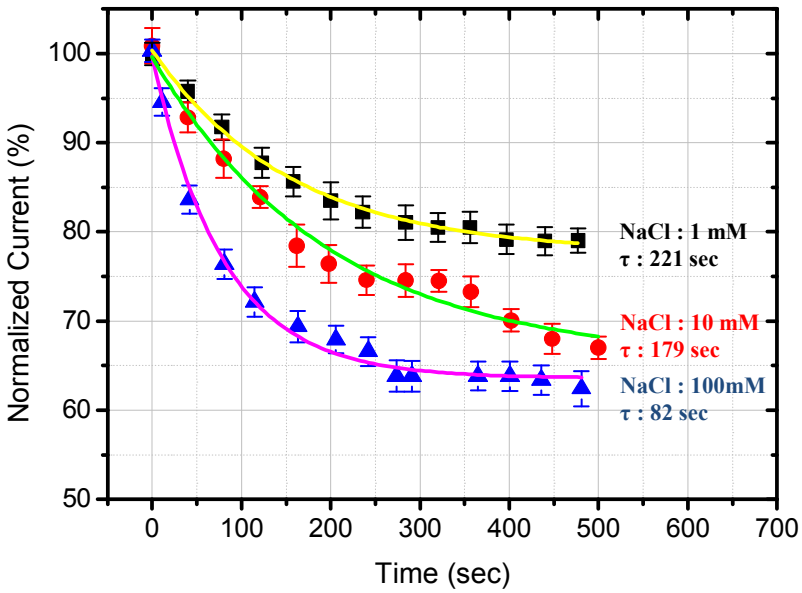

Fig. 3-3. The effect of concentration of electrolyte. Real-time conductance change during DNA hybridization for various salt concentrations (NaCl: 1 mM, 10 mM and 100 mM).

3.2.3 Effects of gold nano particle size

In order to see how the LOD of the device was affected by the GNP sizes, devices with different GNP sizes (*i.e.* with different annealing temperature) were prepared for DNA hybridization experiments. Fig. 3-4 (a) shows SEM images of the GNPs before, and after, the annealing process. The average diameter of the GNP on swCNT network deposited using the thermal evaporator deposition method was originally 8.98±0.31 nm before annealing, but its size increased to 11-13 nm, after annealing at different temperatures. The average diameter of GNP sizes as a result of annealing at 250, 350 and 450 ^{o}C were measured to be 11.97±0.76, 13.09±0.69 and 13.67±0.52 nm, respectively, as shown in Fig. 3-4 (b). Based on the result of the experiment, it was observed that there was no significant difference in the LOD and dynamic range, compared to the device without any additional annealing treatments (*i.e.* device with smaller GNP size), as shown in Fig. 3-4 (c). We mainly used GNPs annealed at 350 ^{o}C for the entire experiment.

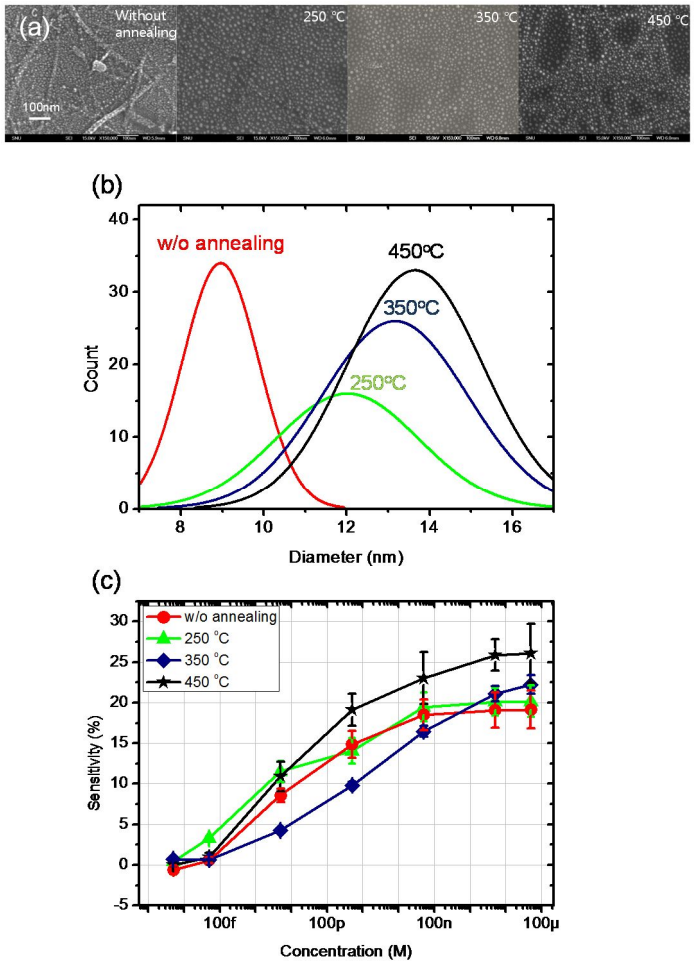

Fig. 3-4. (a) SEM images, and (b) size variation of GNP, as a function of annealing temperature from 250 °C to 450 °C. About 50 GNP diameters for each device were randomly measured (w/o annealing: 8.98 nm, 250 °C: 11.97 nm, 350 °C: 13.09 nm, 450 °C: 13.67 nm). (c) The LODs of DNA hybridization as a function of annealing temperature. Each measurement was done more than 5 times, with 5 different devices.

A literature survey about the particle sizes obtained as a result of two Au deposition methods (electrochemical method, thermal evaporation method) are summarized in Table 3-1. From this it was observed that the average sizes and the standard deviations of GNP by the thermal evaporation method have the similar uniformity compared to those of results using the electrochemical method. The thermal evaporation method has a number of advantages compared to the electrochemical method. For example, it does not require CNT surface modification and is a single-step process with a reduced number of parameters to be controlled and can produce large yields of uncontaminated CNT-nanoparticle composites with good controllability of particle size [42].

Method	Average Diameter (nm)	Standard Deviations (nm)	Reference
Electrochemical	4.41	0.15	[43]
Electrochemical	3.10	0.40	[44]
Electrochemical	1.66	0.38	[45]
Thermal evaporation	7.90	0.30	[42]
Thermal evaporation	8.98	0.31	Our sensor platform

Table 3-1. Average diameter and standard deviation of GNP by electrochemical and thermal evaporation methods

3.3 DNA hybridization under AC biasing

3.3.1 Dengue virus specific sequence DNA detection

In this chapter, we describe the effect of the electrical pulse bias on the detection of charged bio molecules (dengue fever virus-specific DNA sequence) in serum using the CNT integrated bio sensor platform. The dengue fever virus-specific sequence was chosen as the target for this study because of its importance in the detection of dengue fever, a the mosquito-borne tropical disease that is responsible for 3 million infections and 6,000 deaths annually among Southeast Asian men and women [46].

All the chemicals and solvents used in these experiments were of the reagent grade and were used without further purification. The HPLC grade single-stranded DNA samples were purchased from Bioneer, Inc. (Korea). Human serum samples from human male AB plasma (H4522) and PBS (pH 7.6) were purchased from Sigma-Aldrich, Inc. (Korea). The CNN-GNPs linkage chemistry for the dengue fever virus-specific sequence was similar to that used in a previously reported procedure [30]. The p-DNA consisted of 27 base pair oligonucleotides with a thiol group on the 5′ (see Table 3-2) and the thiol group in the p-DNA was linked to the GNP using a well-established thiol chemical method. To immobilize the thiol-modified p-DNA on the GNP, p-DNA was dissolved in the PBS buffer at a concentration of 5 μM. The biosensor chip-integrated CNN-GNPs was exposed to an aqueous DNA solution

(PBS, pH 7.6) for 12 hours at room temperature and then rinsed several times with PBS and deionized water to remove nonspecific bound molecules.

To detect the dengue fever virus-specific sequence t-DNA (see Table 3-2) in the solution (PBS, serum) using pulse measurement scheme, we have performed two experiments: i) an electrical pulse measurement in the PBS, serum with various bias condition (pulse biasing, DC biasing, unbiased) and ii) an optical experiment with the t-DNA optically tagged.

To determine the effect of pulse biasing to this sensor array, DNA hybridization was performed with between the p-DNA complementary to the t-DNA of the dengue fever virus and the noncomplementary DNA as the control as well as the t-DNA. During the hybridization event for 1000 seconds, either pulse bias (±0.5 V at 1 kHz) or DC (0.5V) bias was applied and the normalized currents were measured in the steady state. Fig. 3-5 (a) shows real-time response of hybridization as a function of applying input signal to devices (pulse biasing, DC biasing, unbiased). When the pulse biasing was applied, a large decrease in conductance was observed complementary t-DNA in buffer solution. In contrast, applying a DC bias or unbiased as a control, the device showed a small decrease in the current. The percentage of the current decrease with the DC biasing as compared with the pulse biasing were about a ~14 % and ~30 %, respectively.

It is known that DNA hybridization of t-DNA to the p-DNA on Au electrode result

in a local change in the Au work function [47]. In recent reports, the sensing mechanisms of the DNA sensors based on CNTs have been explained by current modulation resulting from a shift in the energy alignment between the Au contact and the CNT [48, 49]. The DNA immobilization of p-DNA and hybridization with t-DNA on the Au electrode reduces the Au work function and increases the Schottky barrier, thereby increasing the contact resistance and leading to a decrease in the conductance of the devices [30, 32].

The control experiments involving noncomplementary DNA of 5μM were conducted as shown in Fig. 3-5 (b). The pulse bias (±0.5 V, 1 kHz) was applied to the drain electrode during the DNA hybridization between p-DNA and noncomplementary DNA. As compared with the device with the noncomplementary DNA in buffer solution with various input signals (pulse biasing, DC biasing, unbiased), there was no significant difference in the sensitivity and the response time. The sensitivity of the sensor device that has undergone pulse bias was 15 %, whereas the sensitivity of the others (i.e. with DC bias or unbiased) is 14 %~15 %, for 5μM noncomplementary DNA and the time constants from the exponential fitting with the measurement data were about 400s for the pulse biasing, DC biasing.

Compared with the control experiments, the case of complementary DNA hybridization under the pulse-biased condition showed improvements in the sensitivity as shown in Fig 3-5 (c). With the pulse biasing, the DNA hybridization

efficiency was remarkably improved, leading to a faster response and improved sensitivity. Also, the hybridization rates between the probe and target molecules was significantly improved due to the mechanical oscillations of the probe and target molecules caused by the electric field around charged probe molecules [30, 50]

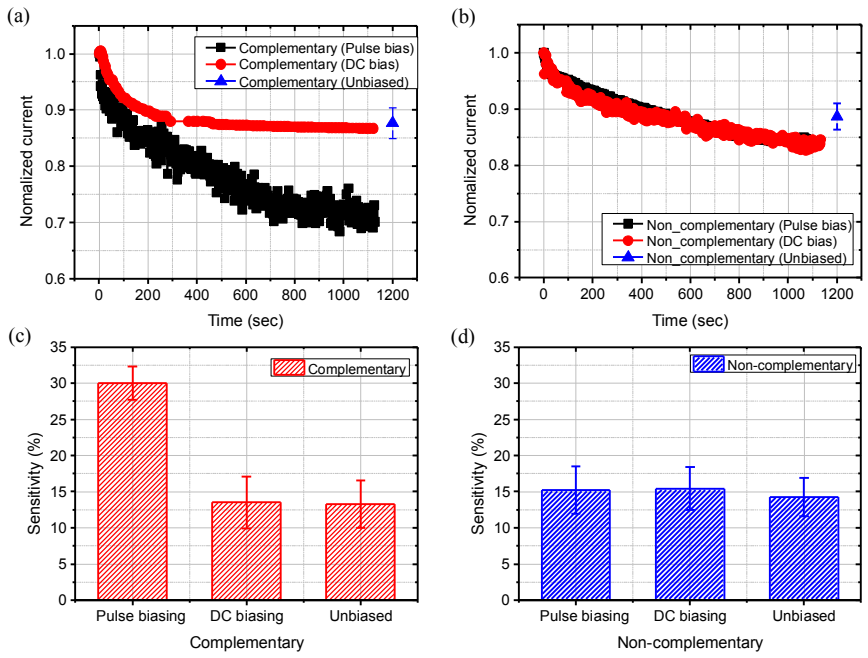

Fig. 3-5. Real-time measurement during DNA hybridization of (a) complementary t-DNA and (b) noncomplementary (NC) DNA, in a buffer solution. Sensitivity data for 3 different biasing conditions applied during hybridization with (c) the complementary t-DNA, and (d) the noncomplementary DNA.

	ss-DNA	Sequences
Probe DNA		5 -HSC6-C12-TCG AGC AAG CCG TGC TGC CTG TAG CTC-C-3
Target DNA	Complementary	5 -GAG CTA CAG GCA GCA CGG CTT GCT CGA-3
	Noncomplementary	5 -TCG AGC AAG CCG TGC TGC CTG TAG CTC-C-3

Table 3-2. DNA sequences used in this study

In order to test the applicability of the electrical pulse measurement scheme in the real PoC applications without the need for washing to remove the nonselectivity bound molecules, we performed the DNA hybridization in serum. After the serum containing complementary t-DNA is applied to the sensor array device, the pulse trains are applied to a specific sensor device, with the other devices remaining unbiased, for comparison. Fig. 3-6 shows the conductance change as the function of the concentration of complementary t-DNA in serum. The sensitivity data were obtained 15minutes after the t-DNA in serum was applied. The current decrease with the unbiased device compared with pulse biasing, (~4 % and ~14 % decrease [t-DNA: 10 μM]), respectively. The sensor device with pulse bias during hybridizations gave a distinct signal sensitivity, whereas the control device without the pulse bias showed no sensitivity other than a noise signal. The sensitivity matches well with the Langmuir equation

$$\frac{\Gamma}{\Gamma_{\max}} = \frac{(K_a c)^{\alpha}}{1+(K_a c)^{\alpha}}, \tag{3.1}$$

with fitting parameters K_a = 1.01×10^9 M^{-1} and α = 0.493, where K_a is an equilibrium constant, c is the concentration of complementary t-DNA, and α is the pseudo-Gaussian distribution of binding energy of set width [51]. The equilibrium constant according to numerical fitting procedures ($O(10^9)$ M^{-1}), agrees well with values reported in literature, (e.g., Knoll et al. [52], Rant et al. [53]) even in serum

condition. In addition, the scheme achieves a signal-to-noise ratio of 2.5 in the detection at 10 pM t-DNA concentration.

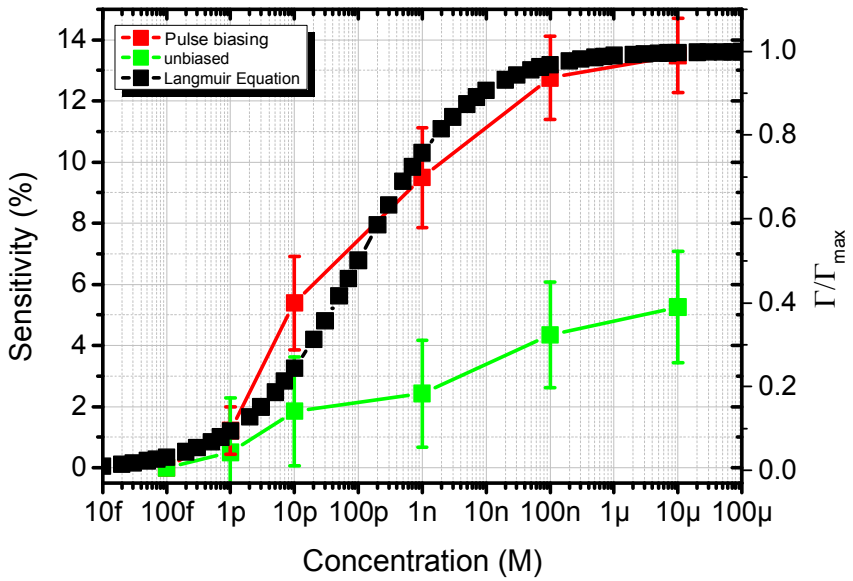

Fig. 3-6. Sensitivity *vs.* t-DNA concentration in serum. Red data; hybridized under the pulsed bias condition. Green data; hybridized under the unbiased condition. Black data; Langmuir fit to the data with the pulsed bias condition. Pulse biasing during hybridization led to a remarkable improvement in sensitivity.

To directly confirm the effect of pulse basing during hybridization in serum, Cy-5-labeled t-DNA (excitation: 650nm, emission: 670nm) was employed. For hybridization the device with the immobilized p-DNA on the CNN-GNP was exposed to a serum containing the labeled t-DNA (5 μM) for 15 minutes at room temperature. After the hybridization under various bias conditions (pulse bias, DC bias), unbound t-DNAs were washed away using the buffer solution and then dried with nitrogen gas. Image were obtained on the metal and in the gap between the electrodes with a confocal laser scanning microscope (Leica Microsystems) using a 20× lens (NA 0.7) with an excitation wavelength of 633 nm and an emission filter range from 675 to 700 nm. Fig. 3-7 show a confocal microscopic image of a device bearing Cy-5-labeled DNA. Only the device for which pulse biasing (Fig. 3-7 (a)) was applied during hybridization significantly enhanced fluorescence toward corresponding dyes, whereas the device for which DC biasing (Fig. 3-7 (b)) was applied during hybridization produced a minimal increase in fluorescence. As a control experiment (Fig. 3-7(c)), an image of the bare device was also obtained, and no significant fluorescence enhancement was detected. The results of the experiments shown in Fig. 3-6 and 3-7 clearly confirmed that the pulse train can indeed enhance the selectivity of the CNT-based electrical DNA sensor.

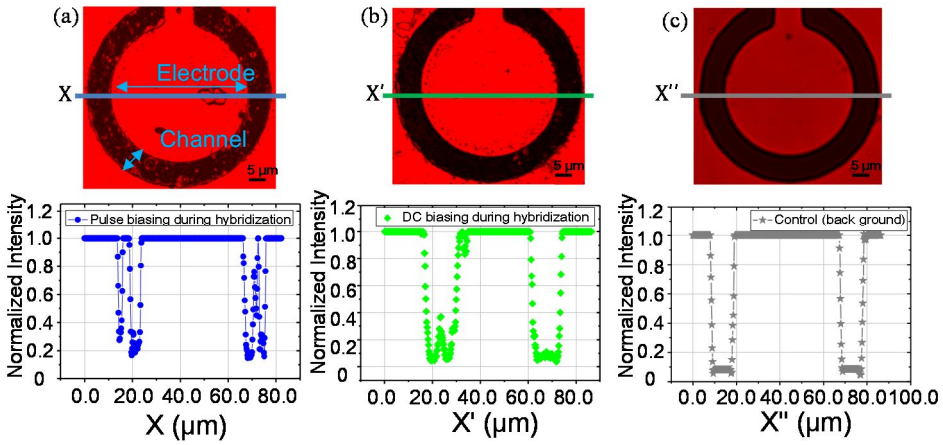

Fig. 3-7. Hybridization of Cy-5-labeled t-DNA. Confocal micrograph of the devices applied by (a) pulse biasing and (b) DC biasing during hybridization. (c) Confocal micrograph of the bare device (for control experiment).

3.3.2 Sensing mechanism in terms of Au work function

It is known that hybridization of t-DNA to the p-DNA on the Au electrode results in a local change in the Au work function as schematically shown in Fig. 3-9 [54-56]. The DNA immobilization of p-DNA and hybridization with t-DNA on the Au electrode reduce the Au work function and increase the Schottky barrier, thereby increasing the contact resistance and leading to a decreasing the conductance of the devices [32].

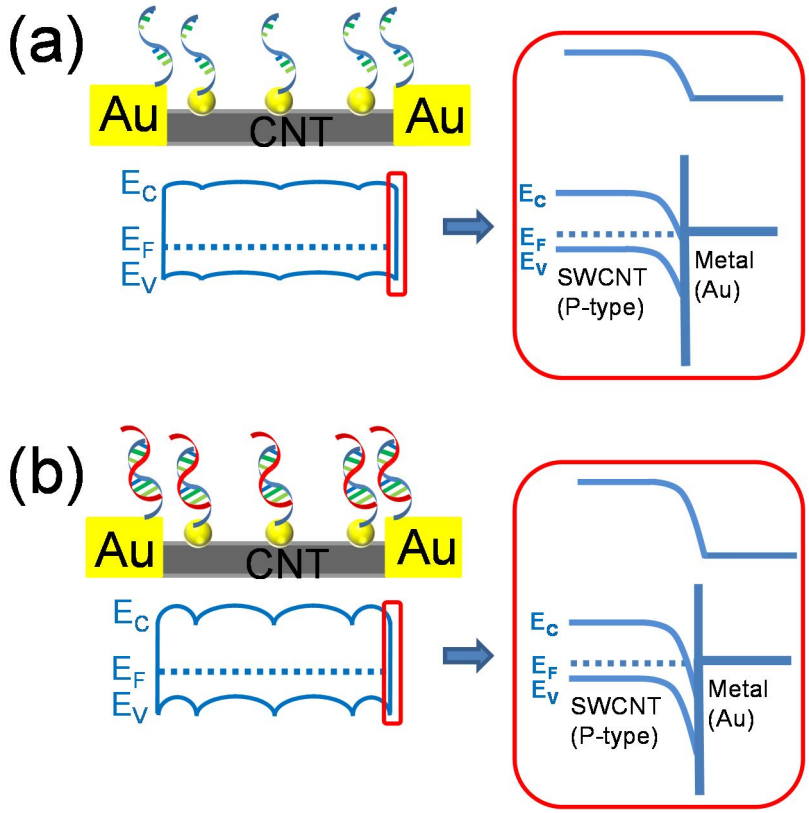

Fig. 3-8. Schematics and corresponding energy band diagram of the device. The work function of Au is decreased by DNA hybridization. (a) The Schottky barrier increases and the hole carriers are depleted. (b) The conductance through CNT decreases due to the reduction of Au work function. (E_C [Conduction band]: An energy band in which electrons can move freely in a solid, producing net transport of charge, E_V [Valence band]: The highest electronic energy band in a semiconductor which can be filled with electrons, E_F [Fermi level]: The energy level at which the Fermi-Dirac distribution function of an assembly of fermions is equal to one-half).

3.4 Conclusion

In summary, the selectivity enhancement method adopting the pulse bias scheme was introduced and experimentally verified by the detection of DNA (dengue fever virus specific sequence) using the CNN-GNP FET sensors. The oscillating motion of the negatively charged p-DNA with pulse bias enhanced the molecular reaction rates and equilibrium binding affinities. Thereby, the hybridization rate constant k_h was increased about threefold, as compared with the unbiased conditions. Also, it was shown that a LOD of as low as ~ pM concentration can be achieved, in the detection of DNA (dengue virus specific sequence) in the serum conditions. Therefore, these results show general applicability of this method, and could open up opportunities in early-stage disease detection and for protein analysis.

Chapter4

The electrical passivation: concepts and simulation

4.1 Introduction

The binding efficiency of specific binding or nonspecific binding is dependent on various environmental factors such as pH, temperature, the ionic strength, the properties of the bio molecule and the nature of the solvent [57, 58]. Among the factors that govern binding are the electrostatic interaction forces between the charged probe and target [59, 60]. When probe molecules are charged, electrostatic interaction plays an important role because target molecules are also charged (depending on the solution pH and isoelectric point [pI] of bio molecules). A maximum in the binding amount could be found around the pI of the bio molecules

[61, 62]. This could be because on the pI, the electrostatic repulsion of biomolecules reach a minimum. Hence, to understand the modulation of the electrode surface pH ($pH_{surface}$) is important for enhancing the selectivity of the electrical biosensor.

In the next section, we propose a modulation of surface pH based on "step pulse biasing", where the hydrogen ion distribution near surface can be controlled in buffer solution applying positive or negative step pulse voltage across the electrodes, in our case, the source and drain. In order to verify the idea, the transient simulation using the numerical simulators developed in-house and the measurements applied to the pH sensor platform were performed.

4.2 Simulation of the modulation of local pH by the electrical pulse

4.2.1 Governing equations for simulation

For the physical model of the binding event at the electrode-electrolyte surface, the transport of ions in the electrolyte and their kinetics are coupled with the Poisson equation as follows in 1 dimensional space.

In the electrolyte solutions, the movement of ion carriers is governed by the drift and diffusion similar to the transport of the electrons and holes in the semiconductor. Accordingly, the continuity equation of ion and the flux are represented by

$$\frac{\partial[n^{\pm}]}{\partial t} = -\nabla \cdot \boldsymbol{F}_{\boldsymbol{n}^{\pm}} = -\nabla \cdot \{\pm\mu_{n^{\pm}}[n^{\pm}]\nabla\psi - D_{n^{\pm}}\nabla[n^{\pm}]\}, \quad (4.1)$$

where $\mu_n^{\pm}$ and $D_n^{\pm}$ are the mobility and the diffusion coefficient of the ions considered in this work.

The electrical potential and ions in the electrolyte solution are governed by the Poisson equation as

$$\nabla \cdot \varepsilon(-\nabla\psi) = q([n^{+}] - [n^{-}]), \quad (4.2)$$

where ε is the permittivity of the electrolyte solution, ψ is the electrical potential, and $[n^+]$ and $[n^-]$ are the concentration of the ions considered in this work including cations (Na^+, K^+, H^+) and anions (Cl^-, OH^-, HPO_4^{2-}, H_2PO^{4-}) in the electrolyte solution. The simulation parameters such as mobility and reaction constants are summarized in Table 4-1 and Fig. 4-1 [63-65].

The electrical potential ψ_0 is applied to the electrode as a Dirichlet boundary condition with respect to bulk solution which is grounded by the reference electrode. For the simulation, the above electrostatic and transport equations are solved self-consistently including the chemical reactions of the following cases: i) no buffer reaction, ii) a PBS solution, iii) CNT defect.

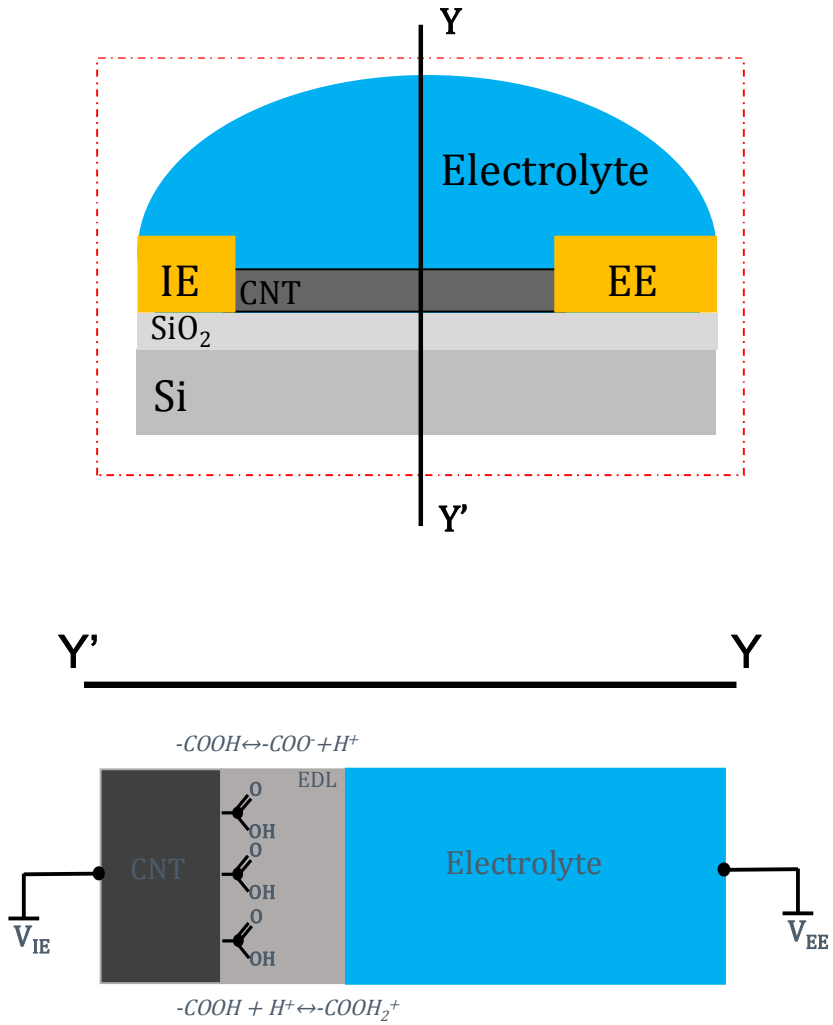

Fig. 4-1. One-dimensional simulation condition. The electrical voltage bias V_{IE} is applied to the electrode.

Parameter	Value	Note	Reference
ε_w	$78\times\varepsilon_0$	Aqueous solution in room temperature	-
μ_{H+}	33.3×10^{-4} cm^2/V-s		[63]
μ_{OH-}	18.8×10^{-4} cm^2/V-s		[63]
μ_{Na+}	5.9×10^{-4} cm^2/V-s		[63]
μ_{Cl-}	7.0×10^{-4} cm^2/V-s		[63]
μ_{K+}	8.6×10^{-4} cm^2/V-s		[63]
$\mu_{H_2PO_4^-}$	3.83×10^{-4} cm^2/V-s		[63]
$\mu_{HPO_4^{2-}}$	3.03×10^{-4} cm^2/V-s		[63]
$D_{n\pm}$	$\mu kT/q$	Einstein relation	
d_H	5 Å	Thickness of Helmholtz layer	
Na^+	1.39×10^{-1} M		
Cl^-	1.39×10^{-1} M		
K^+	4.7×10^{-3} M		
$H_2PO_4^-$	2×10^{-3} M		
HPO_4^{2-}	1×10^{-2} M		

-COOH	$5.6\times10^{12}/cm^2$	Defect site on CNT	[64-66]

Table 4-1. Values used for variables and constants used to calculate the theoretical value

4.2.2 Ion distribution in unbuffered solution

In a solution without addition of a buffer, as a simplest case, only the species H^+, OH^-, Na^+ (0.1 M), Cl^- (0.1 M) contribute to the current transport. Fig. 4-2 shows the theoretical ion distribution (H^+) *versus* the time after applying step pulse voltage for unbuffered solutions under positive (0.5 V) and negative (-0.5 V) bias conditions. In the case of a positive bias (Fig. 4-2 (a)), the positive charged ion (H^+, Na^+) are swept away and the negatively charged ion (OH^-, Cl^-) are congregated at the near surface region (within 0~4 nm) by a high external electric field due to the extended electric double layer on transient state after pulse bias. The other way, in the case of a negative bias (Fig. 4-2 (b)), the negatively charged ions are swept away and the positively charged ions congregated. Since unbuffered solutions are unable to compensate the generation/recombination of H^+ unlike the buffer solution, the ion distribution shows the steep slope of the H^+ concentration in the diffuse layer on steady state. So, the surface pH can be altered quite easily by applying bias.

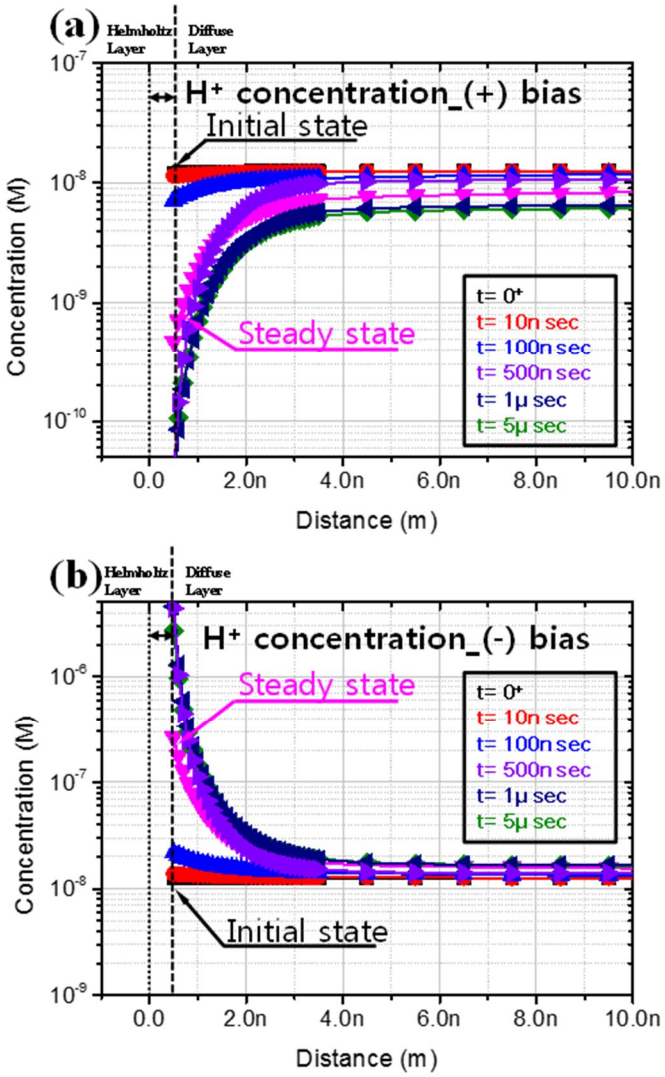

Fig. 4-2. Simulation results on H^+ distribution *vs.* distance from surface after unit pulse is applied in unbuffered solution (H^+, OH^-, Na^+, Cl^-) of pH 7.8 for positive bias (a) and negative bias (b).

4.2.3 Ion distribution in buffer solution (phosphate buffered saline)

For the PBS solution, the interaction between buffers and water are included in the model which can be written as

$$H_3PO_4 \underset{K_{a1}}{\longleftrightarrow} H_2PO_4^- + H^+ \underset{K_{a2}}{\longleftrightarrow} HPO_4^{2-} + 2H^+ \underset{K_{a3}}{\longleftrightarrow} PO_4^{3-} + 3H^+ \quad (4.3)$$

where $H_mPO_4^{n-}$ (n: 0,1,2,3, m: 0,1,2,3) is the phosphate ion and $K_{a1,2,3}$ (K_{a1}: 7.25×10^{-3} M^{-1}, K_{a2}: 6.31×10^{-8} M^{-1}, K_{a3}: 4.80×10^{-13} M^{-1}) are the association constant between phosphate ion and H^+. Note that the reactions between H_3PO_4, PO_4^{3-} and H^+ occur in extreme pH condition. So, the role the reactions by H_3PO_4 and PO_4^{3-} in the diffuse region is negligible and the buffer effect by $H_2PO_4^-$ and HPO_4^{2-} are mainly responsible for the H^+ distribution.

The local concentrations of H^+ in the diffuse layer of a buffer solution is shown in Fig. 4-3 and 4-4 for the positive and negative bias, respectively. For comparison, the H^+ concentration for the unbuffered condition is also depicted in Fig. 4-3 and 4-4. It was shown in the above paragraph that, by applying positive or negative bias to the unbuffered solution, the surface pH is changed to acid or alkaline. But, for a buffer solution condition, the surface pH shows a different result under positive or negative bias. In case of positive bias, the concentration of H^+ near the surface is almost same as the bulk concentration. This is due to the influence of the buffer ion reaction with H^+ via the reaction in Equation (4.3) so that the buffer tries to maintain a constant value for the local pH. However, in case of negative bias, the local ion distribution

for the buffered solution follows the same tendency of that for the unbuffered case. Since the buffer ion concentration on the electrode surface is depleted by the applied bias, the buffer reaction cannot keep the concentration of surface H^+ same as that in bulk case. As a result, the buffer action is lost near the surface under negative bias condition (showing the steep gradient in Fig. 4-4). In summary, even in the buffer solution, the surface pH can deviate from the bulk pH when the pulse bias is applied as shown in Fig. 4-5.

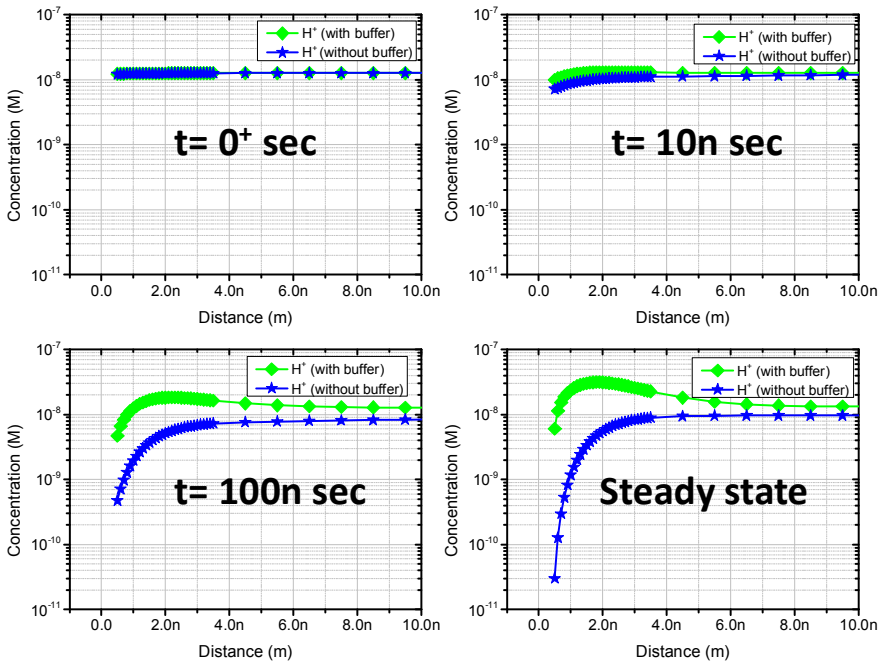

Fig. 4-3. Calculated H^+ distribution representing the surface pH with and without buffer under positive, “with buffer” case is shown in green square and “without buffer” case in blue star.

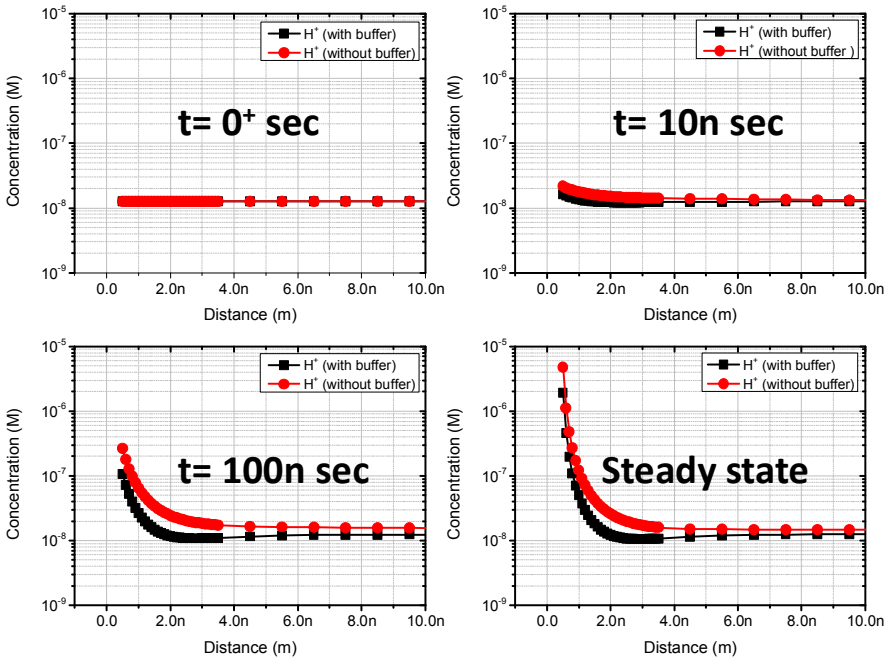

Fig. 4-4. Calculated H^+ distribution representing the surface pH with and without buffer under negative bias, "with buffer" case is shown in black square and "without buffer" case in red circle.

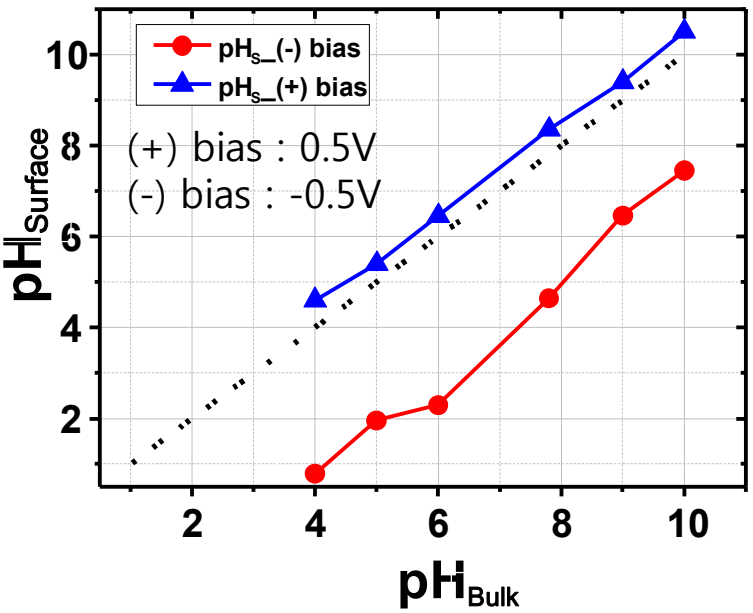

Fig. 4-5. Correlation plot of bulk *vs.* surface pH in buffer solution for two bias conditions: positive bias and negative bias (0.5 V, -0.5 V).

4.2.4 Charging and discharging of the CNT defect (-COOH)

The CNT used in our experiment are treated in HNO_3 for 30 min, and it is estimated that the –COOH group is introduced on the CNT surface [65]. The charge states of the CNT defects (-COOH) are responsible for the CNT conductivity and they are modulated by the H^+, which in turn is modulated by the pulse bias as described above.

The surface reaction can be described as an equation given by:

$$-COOH \underset{K_{a4}}{\leftrightarrow} -COO^- + H^+ \tag{4.4}$$

where –COOH is the defect on CNT, K_{a4} (1.78×10^{-4} M^{-1}) is the association constant between the defect of CNT and H^+ near surface The simulation results on the concentration of COOH on CNT according to the time flow under both positive and negative step pulse condition with various pH solution (pH 3-11) are shown in Fig. 4-6 (a) and (b), respectively. In case of positive bias condition, because the buffer reaction keep the surface pH same as an initial value, the concentration of the COOH are fixed. However, in case of negative bias condition, the COOH at transient state is considerably changed from their initial state. This is because H^+ at the surface accumulates by applying negative bias as in Fig. 4-4 and thus the recombination of H^+ with $-COO^-$ in Equation (4.4) is increased.

Note that the concentrations of COOH under pH 7 reach same steady-state level under the negative bias because all the COO^- are already saturated. This leads to a

pH insensitive characteristic of CNT device, which is experimentally shown in the next section.

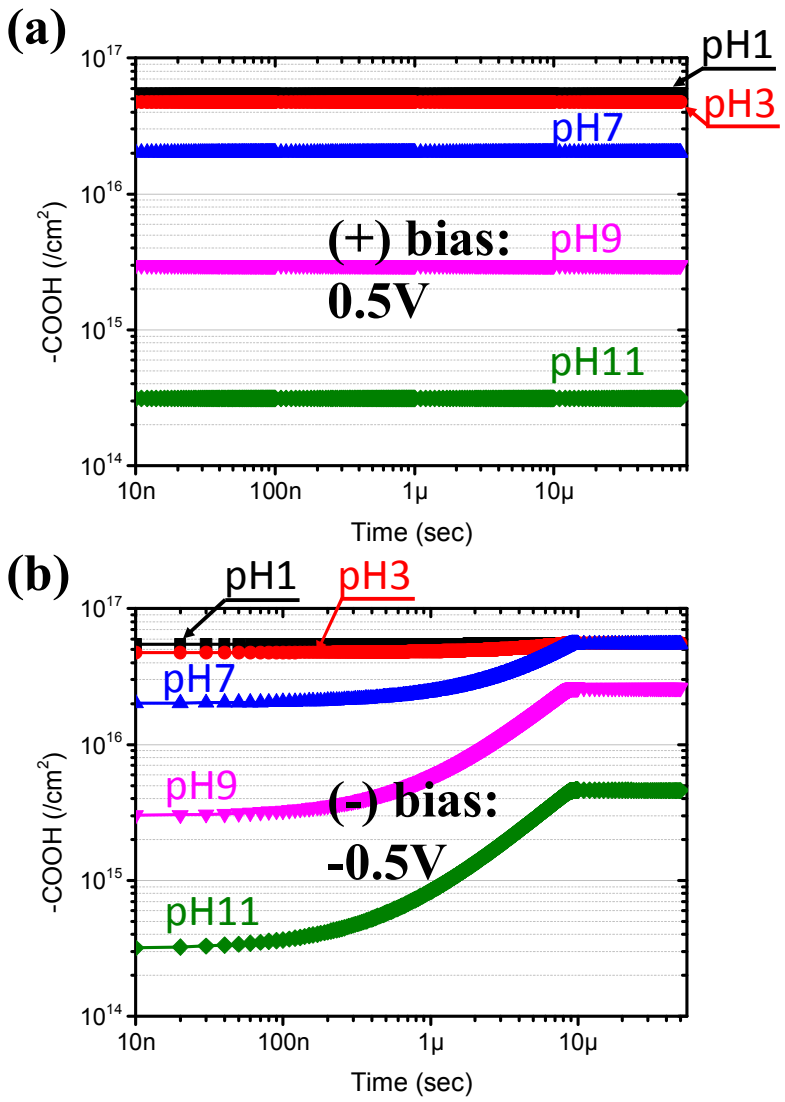

Fig. 4-6. The concentration of the COOH on CNT *vs.* time with various pH solution (pH 3-11) after the unit pulse is applied ((a) positive, (b) negative bias).

4.3 Electrical characteristics of the concentric-shape carbon nanotube network device in pH buffer solution

We have applied the unit step pulse bias measurement scheme to the CNT device and obtain the transient response as shown in Fig. 4-7 under positive (0.5V) and negative (-0.5V) bias. The time required to reach the steady state is determined by the RC time constant, which is related with the mobility and the concentration of the ions within the electrolyte solution. For a 150 mM buffer solution, the RC time constant of our sensor platform is estimated around 4 μsec, in case of 20 μL-droplet.

The current level at the steady-state point in Fig. 4-7 is used to show the relation between the bulk pH and the normalized current of CNT device as shown in the Fig. 4-8 (a) and (b). For comparison, the concentration of COOH from the simulation is also depicted in Fig. 4-8. The normalized current decreases as the pH value increases. This is because, in our CNT device, the current increases as the concentration of COOH becomes higher due to the effect of hole doping [67]. Hence, the lower pH gives higher COOH concentration according to Equation (4.4) and thus gives larger CNT current.

It is worthwhile to notice that the current is insensitive at the acid region (from pH 3 to 7) when the negative bias is applied as shown in Fig. 4-8 (b). It seems to be inadequate considering the pI of carboxyl acid (pI: 3.75) on the CNT and the results from other CNT based pH sensors [68, 69]. However, as aforementioned in the Fig.

4-4, applying negative bias changes the surface pH to acid. So, it can be explained that CNT defect (-COOH) of our devices is fully associated with the acid from pH 3 to 7 as shown in Fig. 4-6 (b) and insensitive as shown in the Fig. 4-8 (b). In other words, even though the bulk pH is within pH 3 to 7, the surface pH becomes less than pH 3 which is below the pI of CNT defect under negative bias so that the CNT device becomes insensitive to pH level of acid.

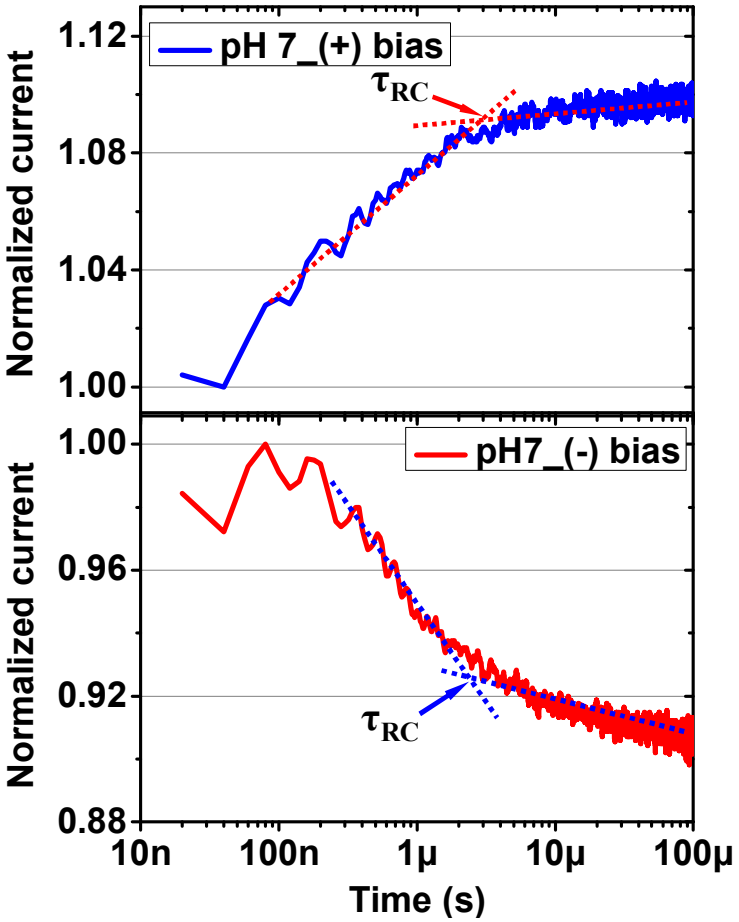

Fig. 4-7. Time *vs.* normalized current curve of the device in the buffer solution (pH7) with various bias condition (positive, negative step pulse bias).

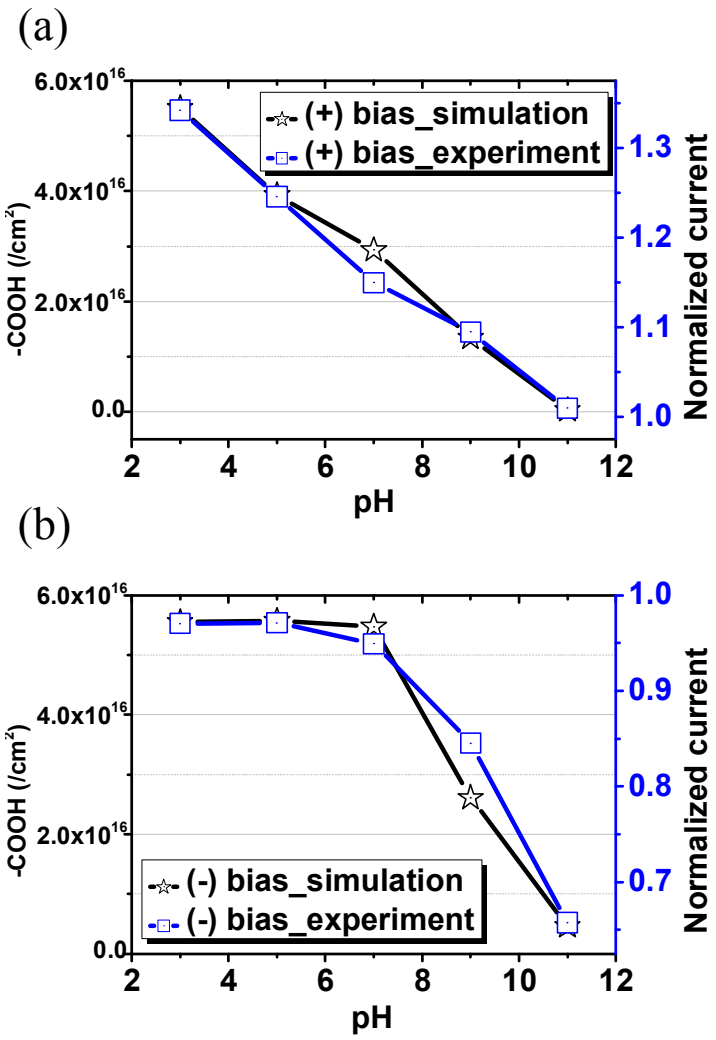

Fig. 4-8. The concentration of the COOH on CNT (simulation result) and the normalized current (experiment result) *vs.* pH after the unit pulse is applied ((a) positive, (b) negative bias). The data denoted by blue line and by black line for the normalized current of device on steady state and the concentration of the COOH, respectively.

4.4 Conclusion

The work provides a detailed description for modelling of a surface and bulk reaction coupled with mass transport of ions in aqueous solution with buffer addition. From the simulation, we showed that the modulation of the surface pH by applying step pulse bias in buffer solution. In addition, the electrical behavior of the CNT device under the step pulse bias with various pH buffer solution is shown. Good agreement between simulation and experiment could be achieved for modulating the local pH by applying bias. The surface pH modulation can be used to enhance the sensitivity and the selectivity for detection of the charged bio molecules such as DNA, RNA and proteins.

Chapter 5

Effects of AC biasing on the electrical passivation

5.1 Introduction

Theoretically, one of the key physical terms which governs the adsorption is an electrostatic interaction forces between the charged surface (the adsorption site) and bio molecule [59] because bio molecules are also charged depending on the solution pH and pI of bio molecules [60]. With the background, we propose a modulation of adsorption ratio based on "pulse train" to change the electrostatic environment at the surface. Under the application of pulse trains across the electrodes, in our case, the source and drain, the H^+ distribution near surface can be controlled in even buffer

solutions. In this way the nonspecific molecules in serum could be electrically passivated and thus it is possible to remove the additional washing steps and further treatments of CNT surface (e.g., Tween-20, PEG, or the like).

In the next following sections, we performed the transient simulation using the numerical simulator developed in–house. To theoretically model the behavior of molecules and ions under the step pulse train, the physics about reaction rate, mass transport and the resulting surface pH-value are considered to solving the Poisson and drift-diffusion equations. In addition, we report the electrical and optical observations for nonspecific binding of biomolecules in serum under the electrical pulse train using the biosensor platform [30].

5.2 Simulation of nonspecific binding of bio molecules

5.2.1 Simulation conditions

For the simulation, the protein is assumed to have a fixed structure with fixed point charges and is embedded in an environment with a high permittivity ε_w representing the solvent as shown in Fig. 5-1. In the continuum with a high permittivity, a charge density represents the ion dissolved in the aqueous solution. Mobile ions are not allowed inside the protein volume and the stern layer [70-72].

Although charged particles can be moved using non-uniform electrical fields, there is not the sole force acting on a particle. The total force on any particle is given

by the sum of many forces including diffusion, electrophoresis and dielectrophoresis force. An electrical field can also induce fluid motion that will drag the particle and the motive forces are electro-osmosis. The magnitudes of these forces can be of the same order as, or in certain circumstances much larger than, the force exerted on the particle by electrophoresis. At certain combinations of frequency, applied voltage and radius of particle, the electrophoresis force can dominates the dielectrophoretic force [73-75].

For small particles (<1 μm diameter) large electrical field gradients are required to produce the forces required to induce motion. We consider that the dielectrophoretic component is much smaller than electrophoretic component and can be negligible, because the amplitude of the applied field was 0.5 V peak to peak and at this amplitude, the threshold electric field of dielectrophoresis ($O(10^5)$ V/cm) [73] is much smaller than the minimum electric field between the two electrode ($O(10^3)$ V/cm)) as shown in Fig. 5-2.

At low concentrations (~500 μM) of bio molecules, the electroviscous effects dominates, and the viscosity of BSA solutions is governed primarily by the net charge on the molecule. Although the attractive interactions are present even in dilute solutions, these are too weak to be of significance [76]. Rather than speculate on the complex inter-molecular particle interactions, we assume that proteins move with a drift velocity. The protein migration is much larger than that for inter-

molecular dynamics.

The mobility of a particle in an electric field is dependent on: i) the strength of the electric field, ii) the dielectric constant of the liquid, iii) the viscosity of the liquid, iv) the zeta potential [76, 77]. To determine the electrophoretic mobility of a particle, the zeta potential can be determine using the Henry Equation:

$$\mu = 2\varepsilon z f(K_\alpha)/3\eta, \quad (5\text{-}1)$$

where μ is the electrophoretic mobility, ε ($78\times\varepsilon_0$) is the dielectric constant, z is the zeta potential, f(K_α) is Henry's function, and η (0.01 g/cm ·s_PBS [NaCl: 0.15 M]) is the viscosity. Henry's function generally has value of either 1.5 or 1.0. The mobility of a "small" particle defined as having radius *r* much smaller than the Debye length of the counterionic atmosphere, *1/k*, is described by the Huckel equation (Henry's equation: 1.0). Also, the electrophoretic mobility of particles of size much larger than the Debye length of the counterionic layer is given by the Helmholtz-Smoluschowski equation (Henry's equation: 1.5) [70]. In this work, the Henry's equation is 1.5 (particle radius: 3.5 nm [albumin], Debye length: <1 nm [NaCl 150 M]) and a relationship for zeta potential as a function of the local pH is summarized in Table 5-1.

It should be noticed that the pH affect the albumin conformation. The normal conformation with the "heart" shape is maintained within pH of 4-8. Below pH 4, the albumin molecule expands and adopts the faster migrating form and the

expanded form at pH < 3.5 [78, 79]. However, in this study, the local pH is varied from 4 to 8 by applying bias condition as shown in Fig. 4-5, the albumin structure maintains normal conformation.

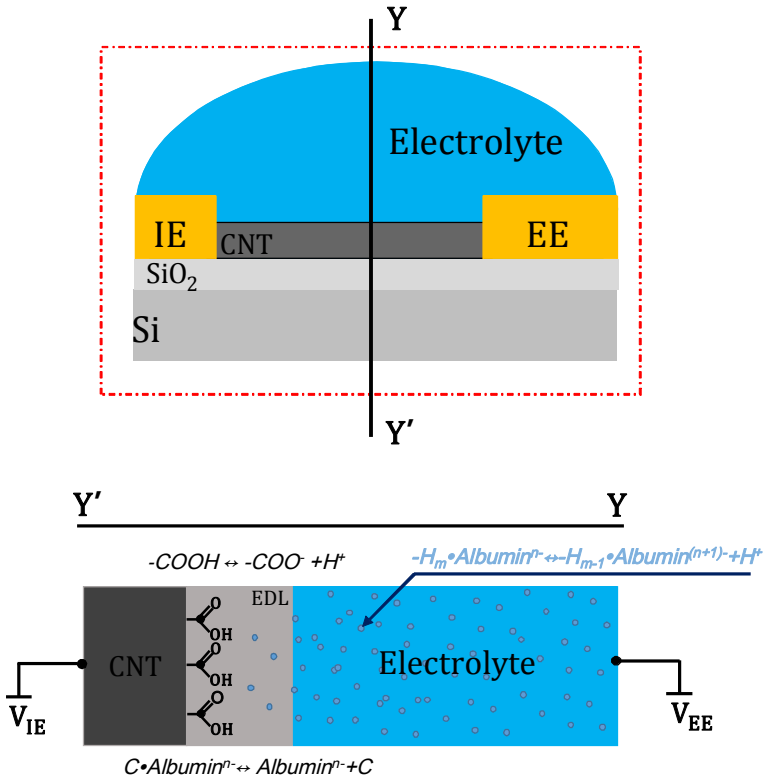

Fig. 5-1. Schematic diagram of the nonspecific binding in the affinity-based biosensor.

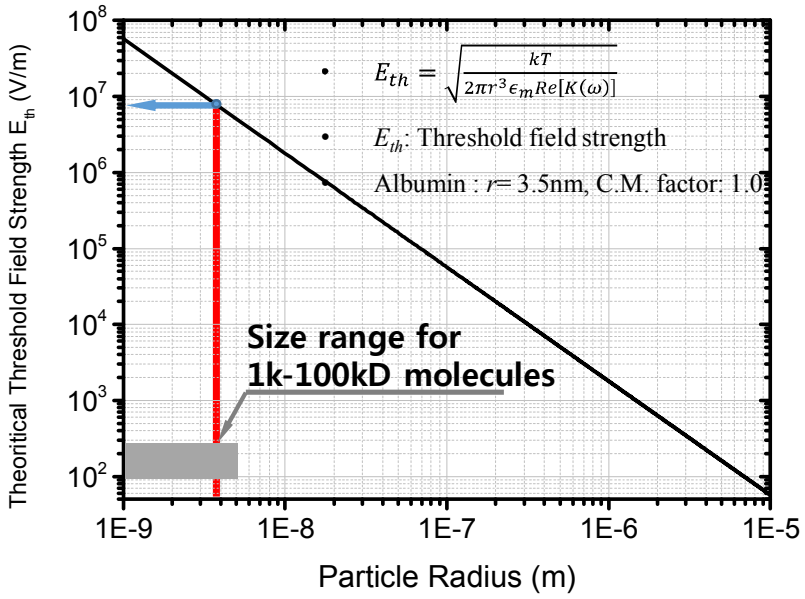

Fig. 5-2. Theoretical threshold field strength of molecular dielectrophoresis.

Parameter	Value	Note	Reference
z	-15.0 mV (@ pH 7)	$z = a \cdot pH_{s1} + b$ *(z: zeta potential, pH_{s1}: surface pH of albumin)* a: -0.00652 b: 0.30644	[76, 77]
Albumin	5×10^{-4} M		
K_{a6}	5.3×10^{5} M^{-1} (@ pH: 7.7)	$K_a = c\times pH_{s2} + d$ *(K_a: association constant (CNT defect-albumin), pH_{s2}: surface pH of CNT)* c: -7.65×10^{5} d: 1.126×10^{6}	[80]
-COOH	$5.6\times10^{12}/cm^2$	Defect site on CNT	[64-66]

Table 5-1. Values used for variables to calculate the theoretical value

5.2.2 Ion distribution in buffer solution (with albumin)

For the simulation of the buffer solution with a nonspecific protein, the protein (albumin) is assumed to be globular [81, 82] with point charges at the center and is embedded in an environment with a high permittivity ε_w ($78\times\varepsilon_0$) representing the solvent.

The charging state of albumin is determined with the reaction as

$$H_2 - Albumin^{n-} \underset{K_{a4}}{\Longleftrightarrow} H - Albumin^{(n+1)-} + H^+ \underset{K_{a5}}{\Longleftrightarrow} Albumin^{(n+2)-} + 2H^+ \quad (5.2)$$

where K_{a4} (7.94×10^5 M^{-1}) and K_{a5} (1.26×10^9 M^{-1}) is the association constant [57] between albumin and H^+. Hence, the charging state of albumin is determined by the concentration of H^+ near the albumin as shown in Fig. 5-3.

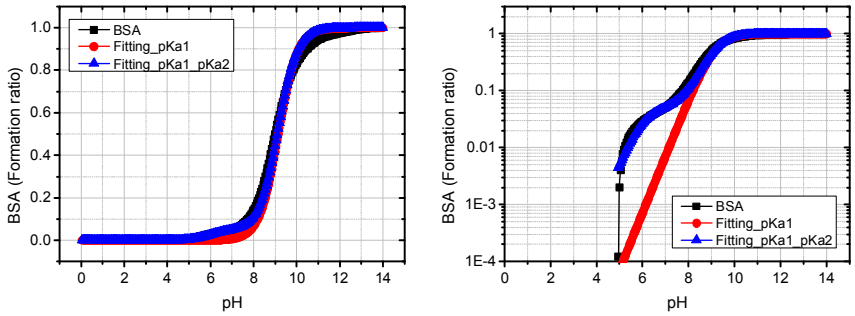

Fig. 5-3. Ionized number of albumin. The surface charge of albumin is fitted well by more than two association constant.

The interaction of the CNT defect (-COO^-) with albumin follows the reaction as

$$C - Albumin^{n-} \underset{K_{a6}}{\Longleftrightarrow} Albumin^{n-} + C \tag{5.3}$$

where C is COO^- (binding site), $Albumin^{n-}$ is the albumin in the electrolyte solution, and K_{a6} (5.3×10^{-5} M^{-1} @ pH:7.7) [80] is the association constant between CNT surface and albumin. Here, the concentration of the binding site is also a function of the surface pH. The system detects the albumin adsorption on CNT surface by the difference of the binding number between before and after the applying pulse train to device.

The suppression of the albumin adsorption on the CNT surface under the application of pulse train is due to the decrease of $Albumin^{n-}$ in Equation (5.3). The decrease of albumin concentration at the surface can be understood from the simulation study in terms of the albumin charging state and surface pH as follows. Before the pulse transition (when the bias stays at high or low level), the buffer reaction and potential difference between the CNT channel and liquid set the H^+ concentration to be its steady-state value as described in Fig. 5-4, 5-5 and 5-6 and the flux of albumin at the surface is negligible because the electric field at the surface is small.

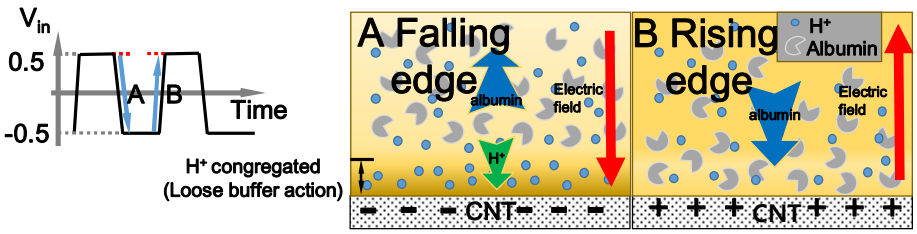

Fig. 5-4. Schematic diagram of the H^+ and albumin in the vicinity of the electrode in an aqueous solution with respect to falling (A) and rising (B) edge of applying pulse train. The pH of the solution can be altered locally by the applying voltage. The surface pH can be lower than the bulk pH with negative bias, and it lead to a less negative charged albumin.

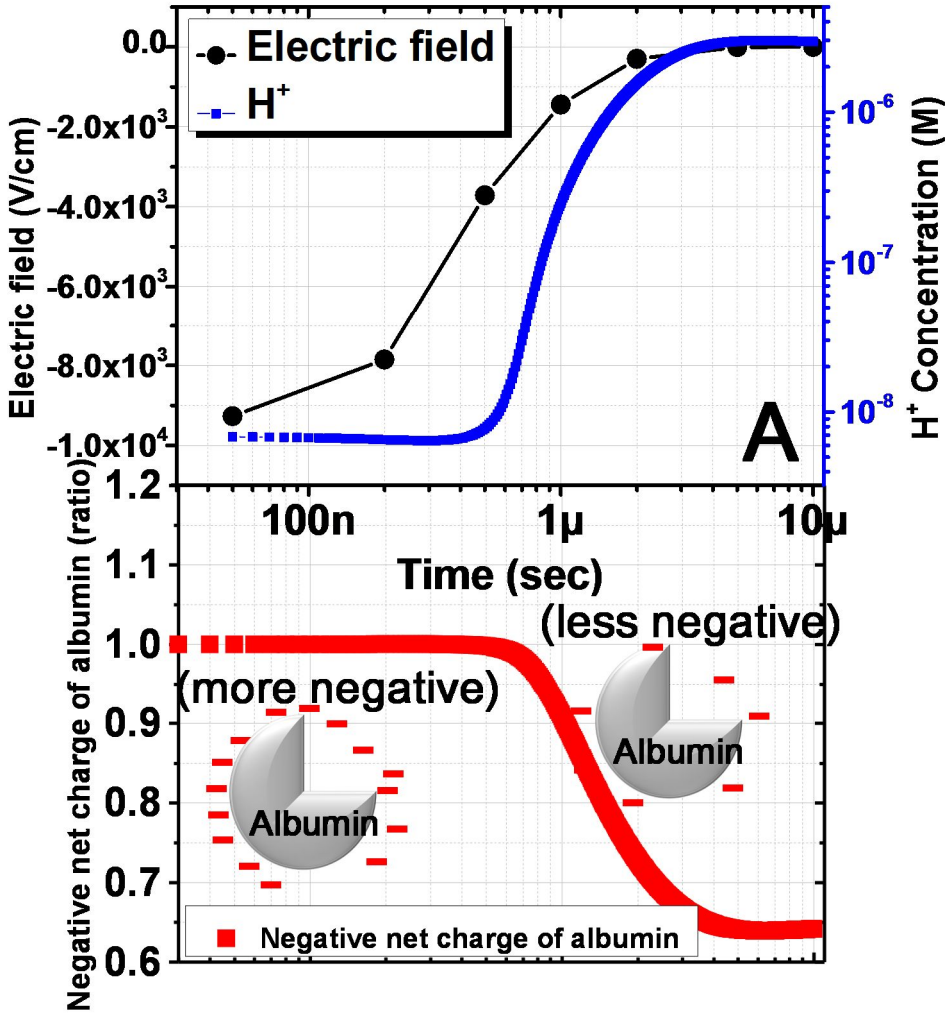

Fig. 5-5. Electric field, H^+ and charging state of albumin profiles in falling edge (A) on transient state. The electrode bias voltage is set to 0.5 V → -0.5 V (falling edge).

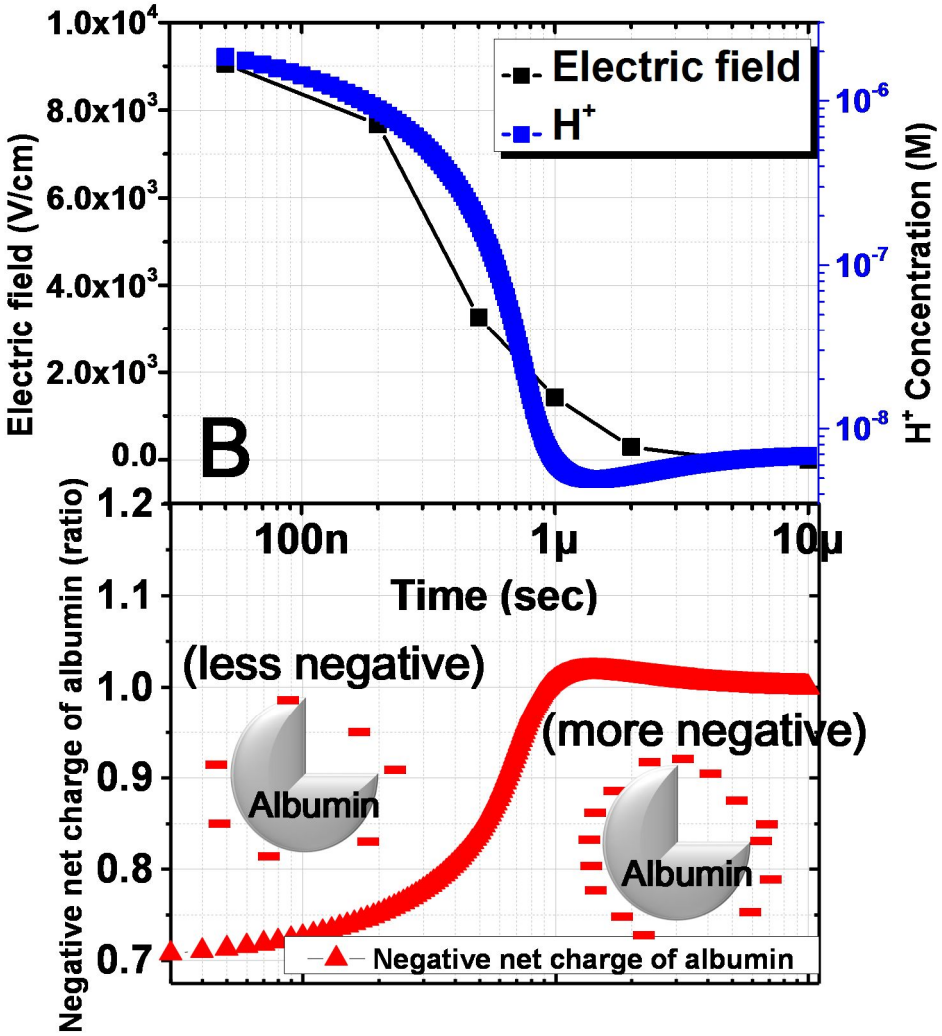

Fig. 5-6. Electric field, H^+ and charging state of albumin profiles in rising edge (B) on transient state. The electrode bias voltage is set to -0.5 V → 0.5 V (rising edge).

However, at the immediate time after step pulse voltage is applied between the channel and the bulk electrolyte solution, the EDL is extended making the high electric field between the channel and bulk of electrolyte within τ_{RC} which can be estimated ~ O(1) micro-seconds when PBS contains 150 mM of NaCl. At this moment, as schematically shown in Fig. 5-4, the H^+ are congregated (A: falling edge) and are swept away (B: rising edge) by high external electric field due to the extended EDL within τ_{RC} after pulse bias. The behaviors of the electric field and τ_{RC} can be confirmed by the simulation result as shown in Fig. 5-5, 5-6.

The point is that the outward flux from the electrode surface at the falling edge is much larger than the inward flux at the rising edge. This is because the charging state of the albumin is different for those two edges. As shown in Fig. 4-5, the application of negative bias changes the surface pH even in the buffer solution and thus H^+ concentrations for falling and rising edge are different. Hence, from Equation (5.2), the net charge of albumin in the vicinity of the electrical channel is changed from more negative to less negative (A: falling edge) and from less negative to more negative (B: rising edge) as shown in Fig 5-5, 5-6. The interesting features of the above result is that the charging state of albumin for the falling edge is different from that for the rising edge and thus the drift terms of albumin in Equation (4.1) for both cases are different. As a result, the more negatively charged albumins at falling edge are more swept away (lager outward flux) but the less

negatively charged albumins are less congregated at rising edge (smaller inward flux) by high external electric field in the transient state within τ_{RC}. Therefore, the concentration of albumin near the surface decreases as the pulse train is applied and thus the albumin adsorption in Equation (5.3) is suppressed.

Fig 5-7 shows the simulation result on the normalized adsorption of albumin as a function of time during the application of pulse trains. At t=0sec, pulse train is applied to the electrode in the buffer condition with the albumin. As shown in the inset of Fig. 5-7, the normalized adsorption of albumin was measured at the rising edges (before the changing the bias) of the pulse train, as denoted with arrows. High external electric field at falling or rising edge induces the unbalanced outward and inward flux of the negative charged albumin on transient state, so that the concentration of adsorbed albumin is decreased as the system experiences the pulse transitions. Therefore, the simulation result in Fig. 5-7 clearly indicates that the pulse train can suppress the albumin adsorption at the CNT surface so that the nonspecific binding can be diminished achieving high selectivity of electrical biosensors.

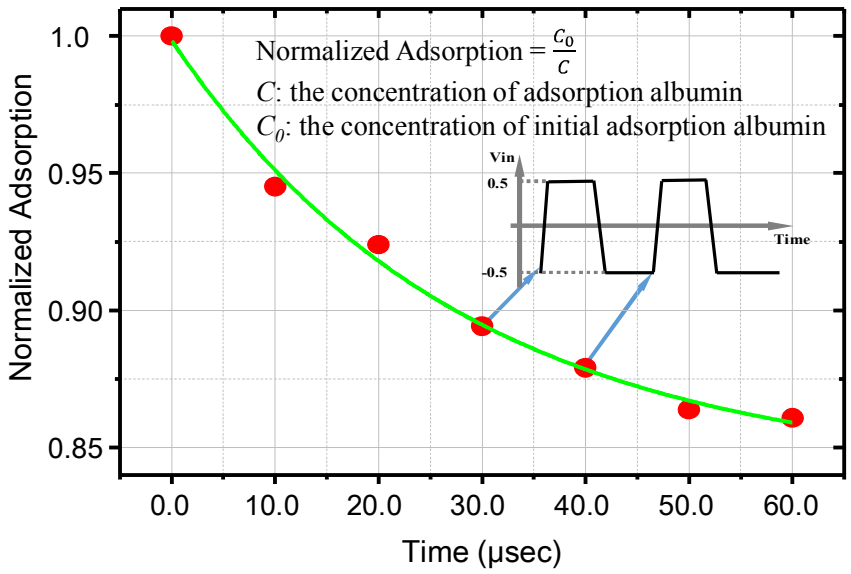

Fig. 5-7. The effect of pulse train to albumin adsorption on CNT. Corresponding adsorption ratio with respect to the time during the application of pulse train. Each points are sampled from the rising edges (inset).

5.3 Experiment; nonspecific binding of bio molecules

As the experiments signatures to support the theoretical simulations in the previous sections, we have performed two experiments: 1) an electrical modulation of CNT channel current in the serum assuming that the modulation is mainly made by the nonselective adsorption of albumin and 2) an optical experiment with the optically tagged albumin.

5.3.1 Modulation of molecules adsorption on CNT's in serum: Electrical experiment

In order to test the applicability of the pulsed bias scheme in the real PoC applications without the washing step to remove the nonselectively bound molecules, the behavior of the CNT current under the serum without the probe-target molecules have been performed.

Fig. 5-8 (a) shows real time characteristics for the DC (0.5 V) and pulse train (±0.5 V, 10 Hz, 1 kHz, 100 kHz) bias on CNN devices after injection of serum. The conductance decrease of the pulse biased device with high frequency (1 kHz, 100 kHz) is 5 %, while that of the DC biased and the pulse biased with low frequency (10 Hz) is approximately 40 %. The real time measurement results less than 10 Hz is almost the same as the case for DC bias and more than 1 kHz shows that the CNN surface is not affected by the nonspecific bio molecules in serum.

Nonspecifically bound bio molecules on the CNN channel gives an effect to the

doping the CNT so that the current is reduced [83]. Also, nonspecifically adsorbed bio molecules between the CNN channel and electrode decreases the transparency of the metal-CNT Schottky barriers [49], thereby reducing the p-type conduction due to changes in the CNT-metal work function difference. However, in pulse train (more than 1 kHz), the pulsed bias induces the interruption of bio molecule adsorption to the CNN surface.

The additional experiments were performed to confirm the effect of the pulse train in serum more clearly. In Fig. 5-8 (b), the real-time responses of the devices under the consecutive pulse train, DC bias (pulse train: 1 kHz, 0.5 V, DC: 0.5 V) are shown. In case of applying pulse train, a slight decrease in conductance was observed after injection of serum, which is consistent with the result in Fig. 5-8 (a). Subsequently, applying of DC bias, the device showed a rapid decrease in the current. Considering the effect of pulse train, the adsorption of albumin is surprisingly small for the sample undergoing the pulse train (1 kHz, 0.5 V), compared with the sample undergoing the DC bias. The dynamic motion of the bio molecules through electric field each moment of signal change from positive bias to negative bias or from negative bias to positive bias suppress the undesired binding event with nonspecific molecules.

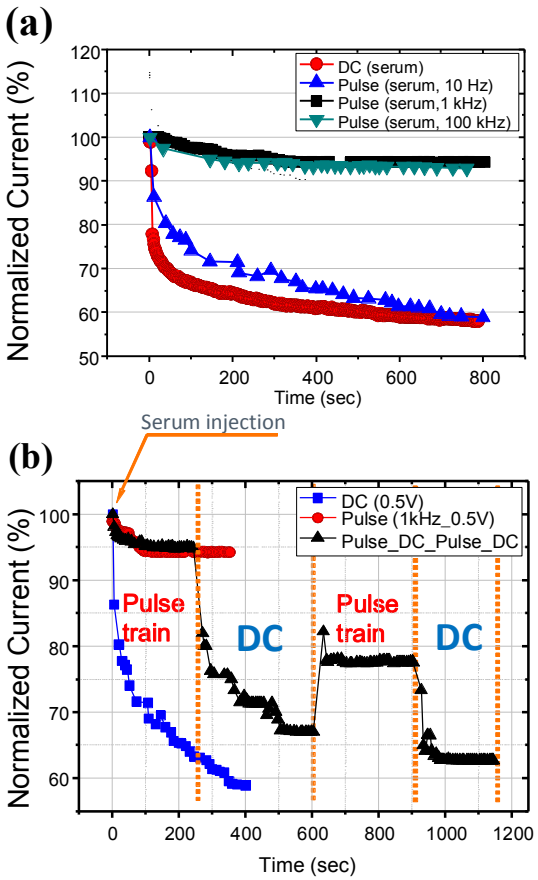

Fig. 5-8. (a) Real-time conductance change upon adding serum under the DC and pulse train conditions with an amplitude of ±0.5 V and frequency of 10 Hz, 1 kHz and 100 kHz. (b) Current *vs.* time for the device with various biasing conditions (Red circles: pulse train with ±0.5 V amplitude and 1 kHz frequency; Blue squares: DC biasing conditions with 0.5 V; Black triangles: consecutive pulse train and DC biasing).

5.3.2 Modulation of molecules adsorption on CNT's in serum: Optical experiment

To directly confirm the effect of pulse train to the nonspecific binding of bio molecules, a fluorescent conjugated albumin (excitation: 650 nm, emission: 688 nm) in PBS solution was employed. For the adsorption, the CNN device was exposed to a buffer solution with fluorescent labeled albumin for 1200 seconds at room temperature. After albumin adsorption under various bias condition (pulse train, DC bias) images were obtained on the metal and in the gap between the electrodes using the confocal laser scanning microscope (Leica Microsystems) using a 20× lens (NA 0.7) with an excitation wavelength of 633 nm and an emission filter range from 675 to 700 nm. In Fig 5-9 (a), the confocal microscopic image of the device undergone the pulse bias during binding with the albumin is shown. Compared with the control device (Fig. 5-9 (b)) without the binding experiment, there is no appreciable difference in the fluorescence intensity implying that the pulse train suppresses the nonspecific binding. However, the device undergone the DC bias (Fig. 5-9 (c)) shows a significant increase in the fluorescence intensity.

From those two experiments in Fig. 5-8 and 5-9, it is clearly confirmed that the pulse train can indeed suppress the adsorption of albumin at the CNT. And, the trend from the experiments is similar to that predicted by the simulation shown in Fig. 5-7. Although the simulation device structure does not directly match with the

experimental one, the agreement in the trend implies the justification of the pulse train method to suppress the adsorption of albumin on CNT surface. It would be tremendous amount work of its own value to develop the simulator considering the three dimensional structure and all the proteins contained in the serum. The purpose of the simulation in this work is to understand the major physical mechanisms responsible for the experimental finding; suppression of the albumin on the CNT surface under the electrical pulse bias condition.

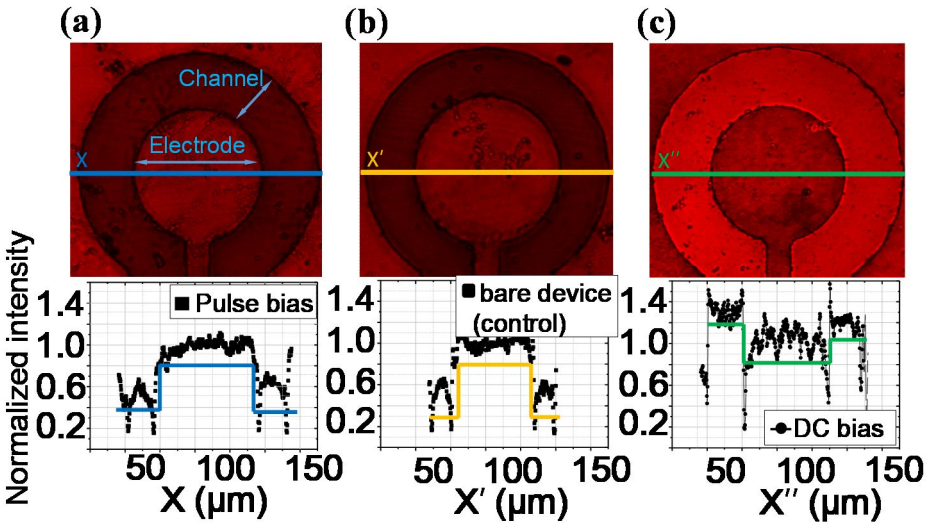

Fig. 5-9. Confocal microscopic image of the devices after nonspecific binding with the fluorescent conjugated albumin; (a) device under the pulse bias (1 kHz, ±0.5 V), (b) the control device without the albumin adsorption experiment, and (c) device under DC bias (0.5 V).

5.4 Conclusion

We have presented a numerical simulation for the response of the nonspecific binding of biomolecules in serum to the pulse train. From the simulation, we showed that the charging state of albumin during the falling edge is different from that of rising edge of the pulse train resulting the reduction of albumin at the surface and thus the nonspecific absorption of albumin is suppressed. In addition, both the electrical modulation of the CNT's and optical measurements under the electrical pulse train suppress the adsorption of charged molecules in serum. The effect may be called the 'electrical washing of nonspecific binding' in the electrical biosensor.

Consequently, it can be concluded that the protein attachment, and not the protein supply, controls the initial adsorption rates. This attachment controlled adsorption process has been previously reported for other protein-surface systems.

Chapter 6

Conclusions

6.1 Summary

In this dissertation, the selectivity enhancement method adopting the pulse-bias scheme was introduced and experimentally verified by detection of the dengue fever virus-specific DNA sequence using CNN-GNP FET sensors. The oscillating motion of the negatively charged p-DNA with the pulse bias enhanced the molecular reaction rates and equilibrium binding affinities. Thereby, the hybridization rate constant k_h was enhanced about threefold, as compared with the unbiased conditions. Also, it has been shown that a limit of detection (LOD) as low as ~pM concentration can be achieved in the detection of DNA in serum conditions.

Modulation of the surface pH by applying step-pulse bias in a buffer solution was also described. In addition, the electrical behavior of the carbon nanotube (CNT) device under the step-pulse bias condition with various pH buffer solutions was

shown. Good agreement between simulation and experiment could be achieved for modulating the local pH by applying bias.

A numerical simulation for the response of the nonspecific binding of biomolecules in serum to the pulse train was introduced. Both the simulation and the experiment, showed that the pulse train could suppress the adsorption of charged molecules in serum, thereby achieving "electrical washing" of nonspecific binding in the electrical biosensor.

6.2 Further Works

In this dissertation, a pulse bias scheme was introduced and enhancement of the sensor performance was achieved, for the detection of DNA hybridization events. In the future, we may expand the present study to include several interesting topics. First, the pulse measurement scheme and the theoretical studies can be extended to sensing the hybridization event for other charged molecules such as proteins. Second, specific uses of the sensor should be investigated to enhance the sensitivity and reliability of the proposed scheme. Finally, to determine the applicability of these results to point-of care analyses, a fully CMOS-integrated CNT sensor array platform should be developed, which would consist of an array of unitary CNT elements, self-reference voltage gating, flexible transducer circuits, and a specialized analog-to-digital conversion scheme.

References

[1] L. Qlark Jr, "Monitor and control of blood and tissue oxygen tensions," *ASAIO Journal,* vol. 2, pp. 41-48, 1956.

[2] L. C. Clark and C. Lyons, "Electrode systems for continuous monitoring in cardiovascular surgery," *Annals of the New York Academy of sciences,* vol. 102, pp. 29-45, 1962.

[3] A. P. F. Turner, "Biosensors--Sense and Sensitivity," *Science,* vol. 290, pp. 1315-1317, 2000.

[4] Z. J. W. Y. W. Lihua and S. S. F. Chunhai, "The Electrochemical DNA Biosensor," *Progress in Chemistry,* vol. 10, p. 015, 2007.

[5] S. Cagnin, M. Caraballo, C. Guiducci, P. Martini, M. Ross, M. SantaAna*, et al.*, "Overview of electrochemical DNA biosensors: new approaches to detect the expression of life," *Sensors,* vol. 9, pp. 3122-3148, 2009.

[6] M. U. Ahmed, M. M. Hossain, and E. Tamiya, "Electrochemical biosensors for medical and food applications," *Electroanalysis,* vol. 20, pp. 616-626, 2008.

[7] M. E. Minaei, M. Saadati, M. Najafi, and H. Honari, "DNA Electrochemical Nanobiosensors for the Detection of Biological Agents," *Journal of Applied Biotechnology Reports,* vol. 2, pp. 175-185, 2015.

[8] C. Chai, J. Lee, and P. Takhistov, "Direct detection of the biological toxin in acidic environment by electrochemical impedimetric immunosensor," *Sensors,* vol. 10, pp. 11414-11427, 2010.

[9] J. J. Gooding, "Biosensor technology for detecting biological warfare agents: Recent progress and future trends," *Analytica Chimica Acta,* vol. 559, pp. 137-151, 2006.

[10] A. Poghossian, A. Cherstvy, S. Ingebrandt, A. Offenhäusser, and M. J. Schöning, "Possibilities and limitations of label-free detection of DNA hybridization with field-effect-based devices," *Sensors and Actuators B: Chemical,* vol. 111-112, pp. 470-480, 2005.

[11] B.-R. Li, C.-W. Chen, W.-L. Yang, T.-Y. Lin, C.-Y. Pan, and Y.-T. Chen, "Biomolecular recognition with a sensitivity-enhanced nanowire transistor biosensor," *Biosensors and Bioelectronics,* vol. 45, pp. 252-259, 2013.

[12] S. Jiang, R. Cheng, X. Wang, T. Xue, Y. Liu, A. Nel*, et al.*, "Real-time electrical detection of nitric oxide in biological systems with sub-nanomolar sensitivity," *Nature communications,* vol. 4, 2013.

[13] A. M. Münzer, Z. P. Michael, and A. Star, "Carbon nanotubes for the label-free detection of biomarkers," *ACS nano,* vol. 7, pp. 7448-7453, 2013.

[14] M. Lee, J. Im, B. Y. Lee, S. Myung, J. Kang, L. Huang*, et al.*, "Linker-free directed assembly of high-performance integrated devices based on nanotubes and nanowires," *Nat Nanotechnol,* vol. 1, pp. 66-71, 2006.

[15] E. S. Snow, J. P. Novak, P. M. Campbell, and D. Park, "Random networks of carbon nanotubes as an electronic material," *Applied Physics Letters,* vol. 82, p. 2145, 2003.

[16] M. A. Topinka, M. W. Rowell, D. Goldhaber-Gordon, M. D. McGehee, D. S. Hecht, and G. Gruner, "Charge transport in interpenetrating networks of semiconducting and metallic carbon nanotubes," *Nano letters,* vol. 9, pp. 1866-1871, 2009.

[17] S. Iijima and T. Ichihashi, "Single-shell carbon nanotubes of 1-nm diameter," *nature*, vol. 363, pp. 603-605, 1993.

[18] E. Stern, R. Wagner, F. J. Sigworth, R. Breaker, T. M. Fahmy, and M. A. Reed, "Importance of the Debye screening length on nanowire field effect transistor sensors," *Nano Lett,* vol. 7, pp. 3405-3409, 2007.

[19] G.-J. Zhang, G. Zhang, J. H. Chua, R.-E. Chee, E. H. Wong, A. Agarwal*, et al.*, "DNA sensing by silicon nanowire: charge layer distance dependence," *Nano letters,* vol. 8, pp. 1066-1070, 2008.

[20] Y. Liu and R. W. Dutton, "Effects of charge screening and surface properties on signal transduction in field effect nanowire biosensors," *Journal of Applied Physics,* vol. 106, pp. 014701-1-014701-8, 2009.

[21] S. Sorgenfrei, C. Y. Chiu, M. Johnston, C. Nuckolls, and K. L. Shepard, "Debye screening in single-molecule carbon nanotube field-effect sensors," *Nano Lett,* vol. 11, pp. 3739-3743, 2011.

[22] Y. Cui, Q. Wei, H. Park, and C. M. Lieber, "Nanowire nanosensors for highly sensitive and selective detection of biological and chemical species," *Science,* vol. 293, pp. 1289-1292, 2001.

[23] M. Pacios, I. Martin-Fernandez, X. Borrise, M. del Valle, J. Bartroli, E. Lora-Tamayo*, et al.*, "Real time protein recognition in a liquid-gated carbon nanotube field-effect transistor modified with aptamers," *Nanoscale,* vol. 4, pp. 5917-5923, 2012.

[24] M. R. Leyden, R. J. Messinger, C. Schuman, T. Sharf, V. T. Remcho, T. M. Squires*, et al.*, "Increasing the detection speed of an all-electronic real-time biosensor," *Lab Chip,* vol. 12, pp. 954-959, 2012.

[25] J. S. Daniels and N. Pourmand, "Label-Free Impedance Biosensors: Opportunities and Challenges," *Electroanalysis,* vol. 19, pp. 1239-1257, 2007.

[26] G. Bhanot, Y. Louzoun, J. Zhu, and C. DeLisi, "The importance of thermodynamic equilibrium for high throughput gene expression arrays," *Biophysical journal,* vol. 84, pp. 124-135, 2003.

[27] S. Sorgenfrei, C. Y. Chiu, R. L. Gonzalez, Jr., Y. J. Yu, P. Kim, C. Nuckolls*, et al.*, "Label-free single-molecule detection of DNA-hybridization kinetics with a carbon nanotube field-effect transistor," *Nat Nanotechnol,* vol. 6, pp. 126-132, 2011.

[28] M. Thompson, L. E. Cheran, M. Zhang, M. Chacko, H. Huo, and S. Sadeghi, "Label-free detection of nucleic acid and protein microarrays by scanning Kelvin nanoprobe," *Biosens Bioelectron,* vol. 20, pp. 1471-1481, 2005.

[29] L. Määttänen, A. Auvinen, U.-H. Stenman, T. Tammela, S. Rannikko, J. Aro, *et al.*, "Three-year results of the Finnish prostate cancer screening trial," *Journal of the National Cancer Institute,* vol. 93, pp. 552-553, 2001.

[30] J. M. Woo, S. H. Kim, H. Chun, S. J. Kim, J. Ahn, and Y. J. Park, "Modulation of molecular hybridization and charge screening in a carbon nanotube network channel using the electrical pulse method," *Lab Chip,* vol. 13, pp. 3755-3763, 2013.

[31] J. H. Cheon, J. Lim, S. M. Seo, J.-M. Woo, S. H. Kim, Y. Kwon, *et al.*, "Electrical Characteristics of the Concentric-Shape Carbon Nanotube Network Device in pH Buffer Solution," *Electron Devices, IEEE Transactions on,* vol. 57, pp. 2684-2689, 2010.

[32] J. W. Ko, J. M. Woo, A. Jinhong, J. H. Cheon, J. H. Lim, S. H. Kim, *et al.*, "Multi-order dynamic range DNA sensor using a gold decorated SWCNT random network," *ACS Nano,* vol. 5, pp. 4365-4372, 2011.

[33] D. W. Kim, G. S. Choe, S. M. Seo, J. H. Cheon, H. Kim, J. W. Ko, *et al.*, "Self-gating effects in carbon nanotube network based liquid gate field effect transistors," *Applied Physics Letters,* vol. 93, pp. 243115-1-243115-3, 2008.

[34] D. R. Thévenot, K. Toth, R. A. Durst, and G. S. Wilson, "Electrochemical biosensors: recommended definitions and classification," *Biosensors and Bioelectronics,* vol. 16, pp. 121-131, 2001.

[35] J. Shi, J. Guo, G. Bai, C. Chan, X. Liu, W. Ye, *et al.*, "A graphene oxide based fluorescence resonance energy transfer (FRET) biosensor for ultrasensitive detection of botulinum neurotoxin A (BoNT/A) enzymatic activity," *Biosensors and Bioelectronics,* vol. 65, pp. 238-244, 2014.

[36] Y. X. Huang, X. C. Dong, Y. X. Liu, L. J. Li, and P. Chen, "Graphene-based biosensors for detection of bacteria and their metabolic activities," *Journal of Materials Chemistry,* vol. 21, pp. 12358-12362, 2011.

[37] R. G. Pearson, "Absolute electronegativity and hardness: application to inorganic chemistry," *Inorganic Chemistry,* vol. 27, pp. 734-740, 1988.

[38] B. J. Hinds, N. Chopra, T. Rantell, R. Andrews, V. Gavalas, and L. G. Bachas, "Aligned multiwalled carbon nanotube membranes," *Science,* vol. 303, pp. 62-65, 2004.

[39] T. Ebbesen, H. Lezec, H. Hiura, J. Bennett, H. Ghaemi, and T. Thio, "Electrical conductivity of individual carbon nanotubes," *nature*, vol. 382. pp. 54-56, 1996.

[40] J. Fuchs, J. B. Fiche, A. Buhot, R. Calemczuk, and T. Livache, "Salt concentration effects on equilibrium melting curves from DNA microarrays," *Biophys J,* vol. 99, pp. 1886-1895, 2010.

[41] D. Irving, P. Gong, and R. Levicky, "DNA surface hybridization: comparison of theory and experiment," *The Journal of Physical Chemistry B,* vol. 114, pp. 7631-7640, 2010.

[42] M. Scarselli, L. Camilli, P. Castrucci, F. Nanni, S. Del Gobbo, E. Gautron, *et al.*, "In situ formation of noble metal nanoparticles on multiwalled carbon nanotubes

and its implication in metal–nanotube interactions," *Carbon,* vol. 50, pp. 875-884, 2012.

[43] Z. Sun, Z. Li, C. Huang, Y. Zhao, H. Zhang, R. Tao*, et al.*, "Ultrasonication-assisted uniform decoration of carbon nanotubes by various particles with controlled size and loading," *Carbon,* vol. 49, pp. 4376-4384, 2011.

[44] S. Bhaviripudi, E. Mile, S. A. Steiner, A. T. Zare, M. S. Dresselhaus, A. M. Belcher*, et al.*, "CVD synthesis of single-walled carbon nanotubes from gold nanoparticle catalysts," *Journal of the American Chemical Society,* vol. 129, pp. 1516-1517, 2007.

[45] S.-Y. Lee, M. Yamada, and M. Miyake, "Synthesis of carbon nanotubes over gold nanoparticle supported catalysts," *Carbon,* vol. 43, pp. 2654-2663, 2005.

[46] D. S. Shepard, E. A. Undurraga, and Y. A. Halasa, "Economic and disease burden of dengue in Southeast Asia," *PLoS neglected tropical diseases,* vol. 7, pp. e2055-1-e2055-12, 2013.

[47] E. L. Gui, L.-J. Li, K. Zhang, Y. Xu, X. Dong, X. Ho*, et al.*, "DNA sensing by field-effect transistors based on networks of carbon nanotubes," *Journal of the American Chemical Society,* vol. 129, pp. 14427-14432, 2007.

[48] Y. Xue and M. Ratner, "Scaling analysis of Schottky barriers at metal-embedded semiconducting carbon nanotube interfaces," *Physical Review B,* vol. 69, pp. 161402-1-161402-4, 2004.

[49] S. Heinze, J. Tersoff, R. Martel, V. Derycke, J. Appenzeller, and P. Avouris, "Carbon Nanotubes as Schottky Barrier Transistors," *Physical Review Letters,* vol. 89, pp. 106801-1-106801-4, 2002.

[50] J.-M. Woo, "Sensitivity enhancement of affinity-based electrical biosensor using pulsed measurement," Ph. D Ph. D, Seoul National University, 2012.

[51] A. W. Peterson, L. K. Wolf, and R. M. Georgiadis, "Hybridization of mismatched or partially matched DNA at surfaces," *Journal of the American Chemical Society,* vol. 124, pp. 14601-14607, 2002.

[52] T. Liebermann, W. Knoll, P. Sluka, and R. Herrmann, "Complement hybridization from solution to surface-attached probe-oligonucleotides observed by surface-plasmon-field-enhanced fluorescence spectroscopy," *Colloids and Surfaces A: Physicochemical and Engineering Aspects,* vol. 169, pp. 337-350, 2000.

[53] U. Rant, K. Arinaga, S. Scherer, E. Pringsheim, S. Fujita, N. Yokoyama*, et al.*, "Switchable DNA interfaces for the highly sensitive detection of label-free DNA targets," *Proc Natl Acad Sci U S A,* vol. 104, pp. 17364-9, 2007.

[54] T. Sumi, H. Wano, and K. Uosaki, "Electrochemical oxidative adsorption and reductive desorption of a self-assembled monolayer of decanethiol on the Au (111) surface in KOH+ ethanol solution," *Journal of Electroanalytical Chemistry,* vol. 550, pp. 321-325, 2003.

[55] X. Cui, M. Freitag, R. Martel, L. Brus, and P. Avouris, "Controlling energy-level alignments at carbon nanotube/Au contacts," *Nano letters,* vol. 3, pp. 783-787, 2003.

[56] R. J. Chen, H. C. Choi, S. Bangsaruntip, E. Yenilmez, X. Tang, Q. Wang*, et al.*, "An investigation of the mechanisms of electronic sensing of protein adsorption on carbon nanotube devices," *Journal of the American Chemical Society,* vol. 126, pp. 1563-1568, 2004.

[57] M. A. Brusatori, Y. Tie, and P. R. Van Tassel, "Protein adsorption kinetics under an applied electric field: An optical waveguide lightmode spectroscopy study," *Langmuir,* vol. 19, pp. 5089-5097, 2003.

[58] T. Kopac, K. Bozgeyik, and J. Yener, "Effect of pH and temperature on the adsorption of bovine serum albumin onto titanium dioxide," *Colloids and Surfaces A: Physicochemical and Engineering Aspects,* vol. 322, pp. 19-28, 2008.

[59] J. Kleijn and W. Norde, "The adsorption of proteins from aqueous solution on solid surfaces," *Heterogeneous Chemistry Reviews,* vol. 2, pp. 157-172, 1995.

[60] O. Moradi, M. S. Maleki, and S. Tahmasebi, "Comparison between Kinetics Studies of Protein Adsorption by Single-walled Carbon Nanotube and Gold Nanoparticles Surfaces," *Fullerenes, Nanotubes and Carbon Nanostructures,* vol. 21, pp. 733-748, 2013.

[61] M. Wahlgren and T. Arnebrant, "Protein adsorption to solid surfaces," *Trends in biotechnology,* vol. 9, pp. 201-208, 1991.

[62] M. Rabe, D. Verdes, and S. Seeger, "Understanding protein adsorption phenomena at solid surfaces," *Advances in colloid and interface science,* vol. 162, pp. 87-106, 2011.

[63] D. R. Lide, *CRC handbook of chemistry and physics*: CRC press, 2004.

[64] J. Chen, M. J. Dyer, and M.-F. Yu, "Cyclodextrin-mediated soft cutting of single-walled carbon nanotubes," *journal of the American Chemical Society,* vol. 123, pp. 6201-6202, 2001.

[65] M. W. Marshall, S. Popa-Nita, and J. G. Shapter, "Measurement of functionalised carbon nanotube carboxylic acid groups using a simple chemical process," *Carbon,* vol. 44, pp. 1137-1141, 2006.

[66] H. J. Kwon, "Electrical Detection of the Microcystin-LR using Carbon Nanotube Network Channel," Ph. D, Seoul National University, 2012.

[67] D. Lee and T. Cui, "pH-dependent conductance behaviors of layer-by-layer self-assembled carboxylated carbon nanotube multilayer thin-film sensors," *Journal of Vacuum Science & Technology B: Microelectronics and Nanometer Structures,* vol. 27, pp. 842-848, 2009.

[68] J. H. Back and M. Shim, "pH-dependent electron-transport properties of carbon nanotubes," *The Journal of Physical Chemistry B,* vol. 110, pp. 23736-23741, 2006.

[69] A. Maroto, K. Balasubramanian, M. Burghard, and K. Kern, "Functionalized metallic carbon nanotube devices for pH sensing," *Chemphyschem,* vol. 8, pp. 220-3, 2007.

[70] B. J. Debusschere, H. N. Najm, A. Matta, O. M. Knio, R. G. Ghanem, and O. P. Le Maître, "Protein labeling reactions in electrochemical microchannel flow:

Numerical simulation and uncertainty propagation," *Physics of Fluids (1994-present),* vol. 15, pp. 2238-2250, 2003.

[71] D. L. Hopkins and V. L. McGuffin, "Three-dimensional molecular simulation of electrophoretic separations," *Analytical Chemistry,* vol. 70, pp. 1066-1075, 1998.

[72] M. Ammam, "Electrophoretic deposition under modulated electric fields: a review," *RSC Advances,* vol. 2, pp. 7633-7646, 2012.

[73] M. Washizu, S. Suzuki, O. Kurosawa, T. Nishizaka, and T. Shinohara, "Molecular dielectrophoresis of biopolymers," *Industry Applications, IEEE Transactions on,* vol. 30, pp. 835-843, 1994.

[74] L. Zheng, J. P. Brody, and P. J. Burke, "Electronic manipulation of DNA, proteins, and nanoparticles for potential circuit assembly," *Biosens Bioelectron,* vol. 20, pp. 606-619, 2004.

[75] A. Nakano and A. Ros, "Protein dielectrophoresis: advances, challenges, and applications," *Electrophoresis,* vol. 34, pp. 1085-1096, 2013.

[76] S. Yadav, S. J. Shire, and D. S. Kalonia, "Viscosity analysis of high concentration bovine serum albumin aqueous solutions," *Pharmaceutical research,* vol. 28, pp. 1973-1983, 2011.

[77] F. Salimi, M. Negahdary, G. Mazaheri, H. Akbari-dastjerdi, Y. Ghanbari-kakavandi, S. Javadi*, et al.*, "A novel alcohol biosensor based on alcohol dehydrogenase and modified electrode with ZrO2 nanoparticles," *Int. J. Electrochem. Sci,* vol. 7, pp. 7225-7234, 2012.

[78] D. C. Carter and J. X. Ho, "Structure of serum albumin," *Advances in protein chemistry*, vol. 45, pp. 153-203, 1994.

[79] E. Edri and O. Regev, "pH effects on BSA-dispersed carbon nanotubes studied by spectroscopy-enhanced composition evaluation techniques," *Analytical chemistry,* vol. 80, pp. 4049-4054, 2008.

[80] A. Javadi, S. Mirdamadi, M. Faghihisani, S. Shakhesi, and R. Soltani, "Well-dispersion of Multi-walled carbon nanotubes in aluminum matrix composites by controlling the mixing process," *Fullerenes, Nanotubes and Carbon Nanostructures,* vol. 21, pp. 436-447, 2013.

[81] F. M. Richards, "The interpretation of protein structures: total volume, group volume distributions and packing density," *Journal of molecular biology,* vol. 82, pp. 1-14, 1974.

[82] H. P. Erickson, "Size and shape of protein molecules at the nanometer level determined by sedimentation, gel filtration, and electron microscopy," *Biological procedures online,* vol. 11, pp. 32-51, 2009.

[83] A. B. Artyukhin, M. Stadermann, R. W. Friddle, P. Stroeve, O. Bakajin, and A. Noy, "Controlled electrostatic gating of carbon nanotube FET devices," *Nano letters,* vol. 6, pp. 2080-2085, 2006.

초 록

바이오 물질의 검출에 있어서 광학적 방식은 검출시간, 크기, 비용 등의 한계를 가지고 있다.

이를 극복하기 위해 다양한 전기적 방식을 적용한 연구가 진행되고 있지만, 혈액 혹은 혈청 내에 존재하는 비 특이 단백질이 감지기의 민감도와 선택도를 저해하는 요인으로 작용하고 있다.

이에 본 논문에서는 실험과 시뮬레이션을 통해 계의 전기화학 반응에 대해 근본적으로 이해하고 이를 이용하여 전기적 방식으로 혈액 혹은 혈청 내의 비 특이 단백질의 흡착을 억제하고 탐침과 특이 분자 간 결합을 증대시킬 수 있는 방안에 대해서 제안하고자 한다.

탐침과 특이 분자 간 결합 효율을 증대시키기 위해서 동심원 구조에 탄소나노튜브를 채널로 이용하는 소자에 특정 조건을 가진 구형파를 인가하였다. 인가한 신호의 주파수와 진폭 그리고 탐침 분자가 고정 되어 있는 금 입자의 크기 및 용액의 농도 등을 조절하여 결합 효율을 최대화 시킬 수 있는 조건을 적용하였다. 또한 실제 적용의 사례로 뎅기 바이러스의 특이 분자를 혈청 조건에서 상당히 낮은 농도의 한계까지 탐지 할 수 있었다.

특정한 조건의 구형파 인가는 혈액 혹은 혈청 내에 존재하는 비 특이 단백질의 흡착을 억제하였다. 단백질의 흡착에 영향을 미치는 환경 요인 중의 하나인 수소 농도를 전기적 신호를 인가하여 임의로 조절하였고, 또한 인가한 신호의 교차점에서 계에 인가되는 전계는 비 특이 단백질의 움직임을 조절하여 흡착에 영향을 미치게 된다. 완충 용액의 이온과 비 특이 단백질의 하나인 알부민의 특성을 고려하여 비 특이 단백질의 흡착 억제를 수치해석적 시뮬레이션과 실험으로 증명하였다.

이러한 실험 방법 및 시뮬레이션은 DNA 뿐만 아니라 특이 단백질의 검출에 있어서도 해당 분자의 전기적 요소를 이용하여 감지기의 민감도 및 선택도를 최대화 할 수 있는 신호 조건을 결정할 수 있는 하나의 플랫폼으로 사용 될 수 있

다.

주요어 : 펄스 측정, 친화도 기반 바이오센서, DNA 혼성화, 수소 농도, 감도.

학번 : 2010-30212